

Slowing Down Forgetting in Continual Learning

Pascal Janetzky

Bosch Center for Artificial Intelligence
Munich Center for Maschine Learning

pascal.janetzky@bosch.com

Tobias Schlagenhauf

Bosch Center for Artificial Intelligence

tobias.schlagenhauf@bosch.com

Stefan Feuerriegel

Munich Center for Machine Learning & LMU Munich

feuerriegel@lmu.de

Abstract

A common challenge in continual learning (CL) is catastrophic forgetting, where the performance on old tasks drops after new, additional tasks are learned. In this paper, we propose a novel framework called ReCL to slow down forgetting in CL. Our framework exploits an implicit bias of gradient-based neural networks due to which these converge to margin maximization points. Such convergence points allow us to reconstruct old data from previous tasks, which we then combine with the current training data. Our framework is flexible and can be applied on top of existing, state-of-the-art CL methods. We further demonstrate the performance gain from our framework across a large series of experiments, including two challenging CL scenarios (class incremental and domain incremental learning), different datasets (MNIST, CIFAR10, TinyImagenet), and different network architectures. Across all experiments, we find large performance gains through ReCL. To the best of our knowledge, our framework is the first to address catastrophic forgetting by leveraging models in CL as their own memory buffers.

1. Introduction

Continual learning (CL) is a paradigm in machine learning where models are trained continuously to adapt to new data without forgetting previously learned information [48, 70]. This is relevant for real-world applications such as autonomous driving [56], medical devices [67], predictive maintenance [22], and robotics [61]. In these applications, the entire data distribution cannot be sampled prior to model training and (fully) storing the arriving data is not possible.

The main challenge of CL is *catastrophic forgetting* [40]. Catastrophic forgetting refers to problems where the performance on old data drops as new data is learned. Catastrophic

forgetting typically happens because prior knowledge is encoded in the combination of the model parameters, yet updating these model parameters during training on new data leads to a change in knowledge and can thus cause the model to forget what it has learned before.

To slow down forgetting, numerous methods have been proposed [14, 25, 27, 32, 35, 38, 39, 52, 53, 69, 76]. Existing methods can be categorized into two main groups [16, 54, 70]: (1) *Memory-based* methods rely on external memory to either store samples from old tasks [e.g., 51, 52] or store separately trained generative networks for generating old data on demand [e.g., 43, 58]. However, this is often not practical due to the fact that CL is often used because streaming data becomes too large and cannot be stored. (2) *Memory-free methods* regularize parameter updates, which may help to slow down forgetting at the cost of learning new concepts more slowly [e.g., 16, 27, 54]. Here, we contribute a different, orthogonal strategy in which we propose to leverage the trained model as its own memory buffer.

In this paper, we develop a novel framework, called *Reconstruction for Continual Learning* (ReCL), to slow down forgetting in CL. Different from existing works, our framework leverages the implicit bias of gradient-based neural network training, which causes convergence to margin maximization points. Such convergence points essentially memorize old training data in the model weights, which allows us then to perform a dataset reconstruction attack. We then integrate this reconstruction attack into CL, where we minimize a data reconstruction loss to recover the training samples of old tasks. Crucially, our framework is flexible and can be used on top of existing CL methods to slow down forgetting and thus improve performance.

We evaluate the effectiveness of our framework across a wide range of experiments. (1) We show the performance gains from our framework across two challenging CL sce-

narios: class incremental learning and domain incremental learning. (2) We compare the performance across different and widely-used datasets, namely MNIST [30], CIFAR10 [2], and TinyImageNet [29] (3) We compare both multi-layer perceptrons (MLPs) and convolutional neural networks (CNNs), finding that consistent performance gains can be achieved across different network architectures. (4) Lastly, we demonstrate the flexibility of our framework by combining our ReCL frameworks with several state-of-the-art CL methods, namely, EWC [27], ER [52], UPGD [16], AGEM [35], LwF [32], and GPM [54]. Here, we find that our framework improves over the vanilla version of the CL methods and can slow down forgetting further. Across all experiments, we find a consistent performance gain from using our ReCL framework.

Contributions:¹ (1) We present a novel CL framework called ReCL to slow down forgetting in CL. To the best of our knowledge, ours is the first method to slow down catastrophic forgetting in which trained models are leveraged as their own memory buffers. (2) We propose to leverage the implicit bias of margin maximization points to create training data in CL. (3) We demonstrate that our ReCL is flexible and that it consistently slows down forgetting.

2. Related Work

Continual learning: CL is a machine learning paradigm where models are trained on newly-arriving data that cannot be stored [70]. In the literature, the following two scenarios are considered especially challenging [21, 63, 65] and are thus our focus. (1) In **class incremental learning** (CIL), a model is trained on new classes that arrive sequentially. Here, each task has a unique label space, and the model’s output layer is expanded to incorporate the new classes. (2) In **domain incremental learning** (DIL), the size of the output layer is fixed, and each task uses the same label space. However, the underlying data that correspond to the labels are no longer fixed but can change over time (e.g., indoor images of cats \rightarrow outdoor images of cats). Later, we apply our framework to both CL scenarios (CIL and DIL) and show that it achieves consistent performance gains.

Forgetting: A main challenge in CL is *forgetting*, also named catastrophic forgetting or catastrophic inference [40, 70]. The problem in forgetting is that, as the model parameters are updated in response to new data, important weights for older tasks are altered and may cause a drop in performance for older tasks [39, 54]. Note that forgetting is a problematic issue in all CL scenarios. [70]. One may think that a naïve workaround is to restrict the magnitude of how much model parameters can be modified during training; yet, this also restricts how new tasks are learned and es-

entially leads to a stability-plasticity tradeoff [70]. Hence, such a naïve workaround is undesired.

To reduce forgetting, several methods have been proposed, which can be grouped into two major categories (see Appendix A for a detailed review). (1) *Memory-based* methods rely on external memory to either directly store samples from old tasks [e.g., 51, 52] or store separately trained generative networks for generating old data on demand [e.g., 43, 58]. A prominent example is experience replay (**ER**) where samples of old data are replayed from a small memory buffer [52]. Another example is **AGEM** [10], which stores old samples to alter the gradient update of subsequent tasks. (2) *Memory-free* approaches do not store old data and can be further grouped into two subcategories. (i) One stream adopts architecture-based approaches, which alter the model architecture to more flexibly accommodate new tasks (e.g., by adding task-specific modules [26, 53, 75]). Oftentimes, these approaches avoid forgetting altogether (by freezing old modules), but at the cost of exponentially growing network sizes. Such approaches usually require task identities and are thus mainly relevant for specific CL scenarios such as task-incremental learning, because of which methods from this subcategory are generally *not* applicable as baselines. (ii) Another stream of approaches regularizes parameter updates so that weights are updated based on their importance for old tasks [27, 54, 78]. Yet, this typically also interferes with learning from new data. Prominent examples are: Elastic weight consolidation (**EWC**) [27], which uses the Fisher information matrix to assess parameter importance and to regularize gradient updates to parameters. Learning without Forgetting (**LwF**) [32] penalizes changes to a model’s output distribution, compared to the beginning of a task, when data from the current task is passed through. (iii) Yet another stream modifies the gradient update through projection methods. An example is gradient projection memory (**GPM**) [54], which computes gradient subspaces that are already occupied by previous tasks. It then uses gradient-preconditioning matrices to guide new gradient updates to be orthogonal. A second example is utility-perturbed gradient descent (**UPGD**) [16], which measures parameter importance by computing the performance difference between unmodified and perturbed weights, and uses this per-parameter utility to control plasticity by scaling a noised gradient.

Difference to generative replay: Our proposed framework is different to both memory-based and memory-free approaches. We do *not* store data of old tasks, and we also do *not* train or keep additional generative networks. Specifically, generative replay uses *separate* generators, which require *additional* training, additional design choices, and an additional labeling network. Even in cases where classifier and generator are merged, such as [64] (they use a VAE and

¹Code: <https://anonymous.4open.science/r/slower-forgetting/>; upon acceptance, we will move the code to a public repository.

apply a reconstruction loss to internal hidden representations and optionally use SI [78] to regularize parameter updates), architectural modifications are necessary. ReCL has four advantages: **(1)** Our ReCL does not require a separate generator. Instead, it uses a custom reconstruction loss to “sample” old data from the classifier network. **(2)** The loss is not based on reconstructed or internal representations. Instead, it optimizes data points so that their derivatives linearly approximate the network weights. **(3)** We do not need to label the reconstructed data, as *the data are already labeled*. **(4)** Lastly, we do not meddle with the network architecture, and also do not alter the learning objective, as this typically interferes with learning new tasks. Rather, we keep the network as-is and combine the reconstructed training data with the current task’s data. Finally, our proposed ReCL is flexible and, as we show later, can be combined with any of the mentioned baselines, where our ReCL leads to further performance improvements.

Dataset reconstruction: The task of dataset reconstruction is related to the idea of memorization in neural networks [7–9]. Specifically, dataset reconstruction builds upon the implicit bias of gradient-based neural network training, which causes neural networks to generalize despite fitting to training-data specific patterns [79]. More technically, Lyu and Li [36] and Ji and Telgarsky [24] show that, despite the freedom to converge to any point during training, homogeneous neural networks are essentially biased toward converging against margin maximization points. Under such a convergence condition, Haim et al. [18] even show that the *entire* training data can be recovered from pretrained binary classifiers without access to any reference data. Buzaglo et al. [8] extend the underlying theory to multi-class networks and general loss functions.

The above-mentioned implicit bias has been studied for regression tasks [3, 4, 44], classification tasks [17, 42, 45], and also different optimization techniques [5, 13, 33, 68]. However, exploiting this implicit bias has *not* yet been studied in CL. Hence, our framework is orthogonal to the above research directions as we leverage dataset reconstruction attacks for CL, which is our novelty.

Research gap: To the best of our knowledge, the implicit bias of gradient-trained neural networks to converge to margin maximization points and thus to memorize training data has been overlooked in CL. Here, we propose to exploit this implicit bias, which enables us to reconstruct training data from machine learning models and which then allows us to slow down forgetting in CL. For this, we develop a novel framework called **Reconstruction for Continual Learning** (ReCL).

3. Problem Statement

We consider the following, standard setup for CL, where data (e.g., images) arrive sequentially and where a model is

updated continually to learn from a series of tasks [46, 53, 54, 76].

Tasks: Each task $\tau \in \{1, 2, \dots, T\}$ has its own data (sub-)set $\mathcal{D}_\tau = (x_i^\tau, y_i^\tau)_{i=1}^{n_\tau} \subseteq \mathbb{R}^d \times C$ with features x_i and corresponding labels y_i from classes $C = \{1, \dots, C\}$. We use the term ‘task’ or ‘time’ interchangeably when referring to τ . Note that the data cannot be stored, meaning that, at time τ , the current dataset \mathcal{D}_τ with $(\mathbf{x}^\tau, \mathbf{y}^\tau)$ is only available for training the current task but cannot be stored. For each task, we have separate train and test split given by \mathcal{D}_τ^{tr} and \mathcal{D}_τ^{te} , respectively.

Network Φ : We train a homogenous² neural network $\Phi(\theta, \cdot)$, which consists of a feature extraction part $\phi_f : \mathbb{R}^d \rightarrow \mathbb{R}^f$ and classification head $\phi_h : \mathbb{R}^f \mapsto C$ (typically, a single dense layer). Together, both ϕ_f and ϕ_h implement an input-output mapping $\Phi(\theta, \cdot) : (\phi_f \circ \phi_h) = \mathbb{R}^d \mapsto C$. We denote the network and its parameters at time τ by Φ_τ . Note that the class of homogenous neural networks is very broad. For example, it includes all vanilla MLPs and CNNs without components introducing “jumps” into the forward pass (such as, e.g., bias vectors or dropout [60]).

Scenarios: We consider the following two common scenarios in CL [for a detailed overview, see 21, 65]. The scenarios vary in how the classification head ϕ_h is used:

1. **CIL:** Each task τ introduces a new set of classes $C_\tau \subset C$. Notably, the label space of any two tasks does not overlap ($C_\tau \cap C_{\tau'} = \emptyset, \forall \tau \neq \tau'$). At each task, the shared ϕ_h is expanded to incorporate the novel classes, while copying the learned parameters from the old output head. Task-identity is only available at train-time.
2. **DIL:** A single shared head is used for each task, but the architecture is not modified upon the arrival of a new τ . Rather, each task introduces new data for already known classes, so that the existing head is simply trained further. Task-identity is available at train-time only.

These scenarios vary in terms of difficulty, and CIL is often considered to be the most challenging one, as novel concepts need to be learned without forgetting old concepts [cf. 21, 65]. **Metrics:** We measure forgetting using the following standard metrics: (i) *average accuracy* (ACC) [35] and (ii) *backwards transfer* (BWT) [35]. ACC captures the accuracy on all tasks up to task T via

$$\text{ACC} = \frac{1}{T} \sum_{\tau=1}^T \text{acc}_{T,\tau}, \quad (1)$$

where $\text{acc}_{T,\tau}$ is the classification accuracy on task τ after training on task T , meaning it gives the averaged test set performance over all tasks. BWT measures the performance loss by contrasting the original task performance with performance after training on subsequent tasks, which thus re-

²See Appendix B.1 for a formal definition.

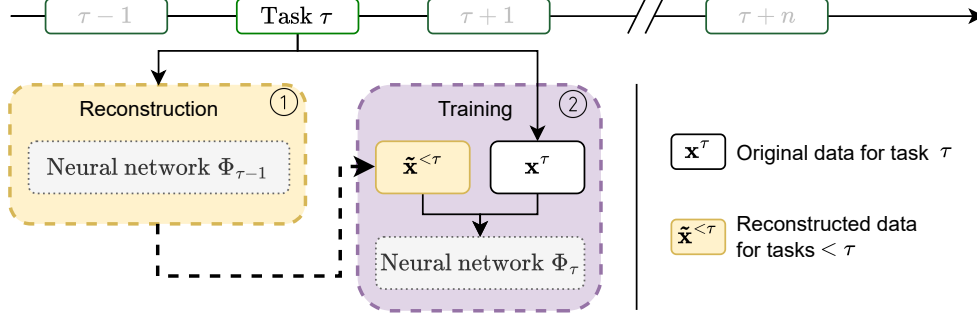


Figure 1. **Overview of our ReCL framework.** Upon the arrival of a new task τ , we reconstruct samples from all previous tasks from the network $\Phi_{\tau-1}$ by minimizing Equation (6). The reconstructed samples are then combined with the current task’s data. Finally, the model is trained on the combined dataset, yielding the new network Φ_{τ} , from which data will be reconstructed in $\tau + 1$.

flects forgetting. Formally,

$$\text{BWT} = \frac{1}{T-1} \sum_{\tau=1}^{T-1} \text{acc}_{T,\tau} - \text{acc}_{\tau,\tau}, \quad (2)$$

where $\text{acc}_{T,\tau}$ is the accuracy on a previous task τ after training on task T , and $\text{acc}_{\tau,\tau}$ is the performance on τ directly after training on τ . For BWT, negative numbers imply forgetting, while positive numbers indicate a retrospective accuracy improvement (which is desired).

Our objective: We aim to *slow down forgetting* in a continually trained neural network Φ that is subject to continual learning. For this, we present a framework where we exploit the implicit bias of gradient-based neural network training towards margin maximization points.

4. Proposed ReCL Framework

In this section, we describe the components of our proposed framework for slowing down forgetting by dynamically extracting the training data of old tasks.

Overview: An overview of our ReCL framework is shown in Figure 1. Our framework performs the following two steps upon arrival of a new task τ . **Step 1: Reconstructing** the training data from $\theta_{\tau-1}$, thus generating the reconstructed data $\tilde{\mathcal{D}}_{\tau} = (\tilde{\mathbf{x}}^{<\tau}, \tilde{\mathbf{y}}^{<\tau})$. **Step 2: Combining** the reconstructed data of previous tasks with the current data $(\mathbf{x}^{\tau}, \mathbf{y}^{\tau})$ and then performing further training of $\Phi_{\tau}(\theta, \cdot)$. Note that both steps are independent of the underlying CL methods, meaning that our framework can be applied on top of *any* existing CL method to slow down forgetting.

Leveraging the implicit bias of convergence to margin maximization points: Our ReCL framework exploits the implicit bias of gradient-based neural network training, which causes neural network weights to converge to margin maximization points [24, 36]. These convergence points are characterized by several conditions [8, 36, 77] which, among others, state that the network weights θ can be ap-

proximated by a linear combination of the network’s gradients on data points x_i . We utilize this finding and optimize *randomly initialized* x_i to closely resemble the training data of previous tasks. We later achieve this by minimizing a tailored reconstruction loss.

4.1. Step 1: Data Reconstruction for CL

For data reconstruction, we perform two sub-steps: (1) We first *randomly* initialize a set of m reconstruction candidates x_i , and (2) we then optimize the candidates to satisfy our objective of reconstructing the training data from old tasks. Both are as follows:

For sub-step (1), we simply initialize m candidates $x_i \sim \mathcal{N}(0, \sigma_x^2 \mathbb{I})$ and set *fixed* labels evenly split across the number of classes.³ That is, $y_i \leftarrow U(C)$.

For sub-step (2), we then optimize the x_i to resemble old data by minimizing a combination of three losses over n_{rec} reconstruction epochs. The losses are as follows: (i) the *reconstruction loss* L_{rec} , (ii) the *lambda loss* L_{λ} , and (iii) the *prior loss* L_{prior} . Here, the reconstruction loss in (i) denotes our central objective: it optimizes the candidates to reconstruct old data. However, to ensure the theoretical foundation of the implicit bias, we must ensure that the network weights can be approximated by a linear combination, for which we need the lambda loss in (ii), which enforces a constraint on the coefficients of the linear combination. To incorporate prior domain knowledge about the reconstructed data (such as having knowledge about its value range), we need the prior loss in (iii). It forces the candidates to lie within (normalized) value ranges. The formal definitions of the different losses are below:⁴

(i) Reconstruction loss: The *reconstruction loss* L_{rec} optimizes the m randomly initialized candidate samples x_i .

³The label information can be derived from the output layer of the trained neural network.

⁴We provide further details on the reconstruction process in Appendix B.

Inspired by Buzaglo et al. [8], we define it as

$$L_{\text{rec}}(x_1, \dots, x_m, \lambda_1, \dots, \lambda_m) = \left\| \theta_{\tau-1} - \sum_{i=1}^m \lambda_i \nabla_{\theta_{\tau-1}} \Phi_{\tau-1}(\theta_{\tau-1}; x_i) \right\|_2^2, \quad (3)$$

where $\|\cdot\|_2^2$ denotes the squared L_2 norm (i.e., squared Euclidean distance), x_i are reconstruction candidates, λ_i are learnable scaling coefficients. The number of reconstruction candidates, m , is a hyperparameter.

(ii) Lambda loss: The *lambda loss* L_λ constrains the scaling coefficients λ_i . It is defined as

$$L_\lambda = \sum_{i=1}^m \max\{-\lambda_i, -\lambda_{\min}\}, \quad (4)$$

where λ_{\min} is a hyperparameter. Note that the λ_i are not part of the old task’s training data, but are necessary for the underlying theory to hold [18] and thus to solve the reconstruction problem defined by Equation (3). We provide further details in Appendix B.2.

(iii) Prior loss: The *prior loss* L_{prior} constrains the value range of the (reconstructed) images to lie within normalized range -1 to 1 . Generally, this loss is used to encode prior background/domain knowledge about the reconstruction data. Here, we follow [18] and use it to restrict that the values of the reconstructed data are in a certain range. Later, in our experiments, we work with images and thus enforce normalization to $[-1, 1]$ by

$$L_{\text{prior}} = \sum_{i=1}^m \sum_{k=1}^d \max\{\max\{x_{i,k} - 1, 0\}, \max\{-x_{i,k} - 1, 0\}\}, \quad (5)$$

where d is the dimensionality of the features x_i .

Overall loss: For each task, we minimize the following overall loss

$$L_{\text{full}} = L_{\text{rec}} + L_\lambda + L_{\text{prior}} \quad (6)$$

using stochastic gradient descend (SGD) over n_{rec} reconstruction epochs. This yields the $\tilde{\mathcal{D}}_\tau = (\tilde{\mathbf{x}}^{<\tau}, \tilde{\mathbf{y}}^{<\tau})$.

4.2. Step 2: Combining the Reconstructed Data for Training

Step 2 now leverages the reconstructed data, $\tilde{\mathcal{D}}_\tau$, when training for the new task τ . We set the number of samples to reconstruct to $m = \sum_{t=1}^{\tau-1} n^t$ and initialize the fixed labels $\tilde{\mathbf{y}}^{<\tau}$ evenly across all classes. We then combine $\tilde{\mathcal{D}}_\tau$ with the current training data $\mathcal{D}_\tau^{\text{tr}}$ and train Φ_τ on the combined dataset.

4.3. In-Training Optimization of Reconstruction Hyperparameters

Our ReCL consists of six hyperparameters, which are primarily used in Equation (3) to Equation (6). The hyper-

parameters are: (i) λ_{\min} constrains the scaling effect of λ_i ; (ii) σ_x controls the initialization of the x_i from a Gaussian distribution; (iii) lr_x and (iv) lr_λ are the learning rates for the SGD optimizers of x_i and λ_i , respectively; (v) n_{rec} is the number of reconstruction epochs; and (vi) m is the number of reconstruction candidates.

The hyperparameters λ_{\min} , σ_x , lr_x and lr_λ are tuned in-training at each task τ . We use three strategies: (1) In the *naïve* strategy, we perform no hyperparameter optimization and simply run n_{rec} reconstruction epochs with default hyperparameters based on related works from computer vision [8, 18]. We select this strategy as our reference when we refer to our ReCL, and consider the following other two strategies as ablations. (2) In the *unsupervised* strategy, we use a Bayesian search at each task to optimize the hyperparameters by minimizing the Equation (6), where each trial runs for n_{rec} epochs. (3) In the *supervised* strategy, we use reference data of old tasks stored in a memory buffer to guide the optimization process. We then maximize the structural similarity index measure (SSIM) [71] between reconstructed data and real reference data. To measure the similarity among images, we follow Buzaglo et al. [8] and, for each real sample, find the nearest generated neighbour using the L_2 distance and then compute the SSIM between closest pairs. Details are in Appendix D.5. As before, we run n_{trials} parameter trials at each task.

Note that hyperparameters n_{rec} and m are not tuned during training but set beforehand. We analyse their influence on ReCL in sensitivity studies.

5. Experimental Setup

We adopt CL scenarios (i.e., CIL and DIL), datasets, and baselines analogous to prior literature [e.g., 14, 16, 27, 55, 65]. We later report ACC and BWT (see Section 3) over 5 runs with independent seeds, where, in each run, we randomly distribute the classes into tasks.

Datasets: We evaluate our ReCL using the split variant of MNIST [30], CIFAR10 [2], and TinyImageNet [14, 29], where the classes are split into sequential tasks for CL. We refer to them as SplitMNIST, SplitCIFAR10, and SplitTinyImageNet, respectively. All datasets are well established for benchmarking in CL research (e.g., [14, 16, 50, 55, 65, 78]). We split the datasets into five non-overlapping tasks (two tasks with 20 classes each for SplitTinyImageNet), and randomly select $n = 100$ training samples per class. We use the entire respective test set for reporting the out-of-sample performance. See Appendix C for further details.

Baselines: We adopt a default baseline where a machine learning model is trained sequentially on each task but without reducing forgetting in any way (named **Finetune**). We further implement six state-of-the-art methods for CL: **EWC** [27], **ER** [52], **UPGD** [16], **AGEM** [35], **LwF** [32], and **GPM** [54].

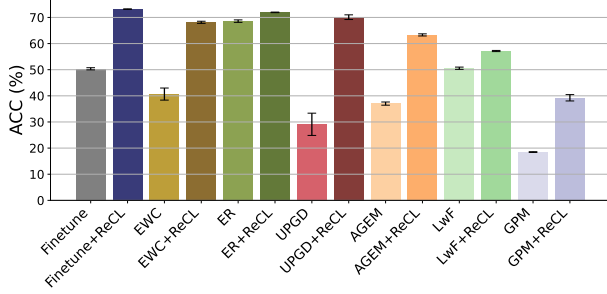


Figure 2. **ACC(↑) for CIL, SplitMNIST:** All methods benefit from our ReCL. Used standalone, ReCL already is competitive to CL methods.

We implement the following variants of our ReCL framework. (i) We report a ReCL-only baseline with a standard machine learning model, but *no* other CL method for slowing down forgetting (named **Finetune+ReCL**). (ii) We further integrate the above CL baselines into our framework, which we refer to as **EWC+ReCL**, **ER+ReCL**, **UPGD+ReCL**, **AGEM+ReCL**, **LwF+ReCL**, and **GPM+ReCL**. Thereby, we demonstrate that our framework can be flexibly used on top of state-of-the-art CL methods. Further, any performance gain between the variant with our framework and the vanilla baselines must then be directly attributed to the fact that our framework successfully slows down forgetting.

Implementational details: We use SGD [6], both for training and for data reconstruction (Equation (6)), where set $n_{\text{rec}} = 100$, $m = n$, and, where applicable, run $n_{\text{trials}} = 100$ trials using Bayesian search with Optuna [1] to optimize the reconstruction hyperparameters during training (*(un-)supervised strategies*). The corresponding hyperparameter grid is given in Appendix B.3. To ensure a fair comparison, we extensively tuned the hyperparameters over the search grid in Appendix D.3. See Appendix D for more details.

Scalability: All experiments are conducted on a single NVIDIA A100 80GB GPU. We report average runtimes in the appendix. The overhead from adding our framework and the default naïve strategy is relatively small. See Appendix K for more details.

6. Results

6.1. Scenario CIL

Main results: The main results are in Figures 2 and 3 and Tab. 1 (further results are in Appendix E). We make the following observations: (1) Our Finetune+ReCL improves over the Finetune baseline by up to 45.37 % (ACC) and 63.11 % (BWT). Hence, even the standalone version of our ReCL framework is competitive. (2) Our proposed ReCL is highly effective: it slows down forgetting (lower BWT) and

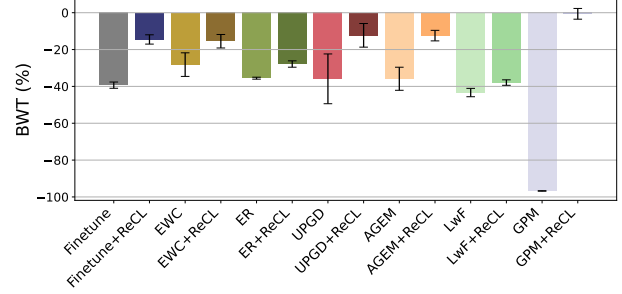


Figure 3. **BWT(↓) for CIL, SplitMNIST:** ReCL strongly reduces forgetting for all methods and is competitive when used standalone.

Table 1. **Scenario CIL:** Results for training a MLP on SplitMNIST and CNN on SplitCIFAR10. Shown: average ACC(↑) and BWT(↓) over 5 random repetitions with varying order and init.

Method	SplitMNIST			SplitCIFAR10	
	ACC(±std)	BWT(±std)		ACC(±std)	BWT(±std)
Finetune	50.34 ± 0.42	-39.33 ± 2.44		15.87 ± 0.14	-71.40 ± 0.77
Finetune+ReCL	73.18 ± 0.09	-14.51 ± 1.64		20.15 ± 0.43	-54.48 ± 1.13
EWC	40.67 ± 2.31	-28.18 ± 16.37		16.05 ± 0.12	-71.13 ± 0.94
EWC+ReCL	68.13 ± 0.41	-15.49 ± 2.19		16.10 ± 4.06	-71.67 ± 0.24
ER	68.59 ± 0.47	-35.54 ± 0.71		21.05 ± 0.04	-62.90 ± 1.09
ER+ReCL	71.94 ± 0.11	-27.85 ± 2.22		22.46 ± 0.27	-57.11 ± 0.77
UPGD	29.10 ± 4.26	-35.89 ± 12.54		15.94 ± 0.13	-71.57 ± 0.21
UPGD+ReCL	70.10 ± 0.90	-12.28 ± 1.73		15.92 ± 0.74	-71.67 ± 0.08
AGEM	37.03 ± 0.61	-35.85 ± 3.23		16.18 ± 0.04	-71.49 ± 0.32
AGEM+ReCL	63.31 ± 0.41	-12.43 ± 3.95		16.12 ± 4.13	-71.28 ± 0.50
LwF	50.56 ± 0.43	-43.34 ± 2.67		19.71 ± 0.74	-53.39 ± 0.53
LwF+ReCL	57.15 ± 0.22	-37.92 ± 1.60		23.59 ± 0.38	-40.65 ± 3.28
GPM	18.48 ± 0.15	-96.75 ± 0.18		14.10 ± 0.45	-68.95 ± 0.36
GPM+ReCL	39.25 ± 1.22	-60.60 ± 0.52		19.56 ± 0.61	-61.12 ± 1.99

improves classification (higher ACC) for *all* baseline methods. Note that we ensured fair comparison by performing extensive hyperparameter tuning for all baselines. Hence, all performance improvements must be attributed to how our framework slows down forgetting.

Sensitivity study. We conduct a sensitivity study where we (i) vary the number of reconstruction samples (default: $m = n = 100$) in the CIL scenario and where we (ii) adopt alternative strategies for tuning the reconstruction hyperparameters. The results are in Figure 4 (further results are in Table 5 in the appendix). We make the following observations: (1) At all numbers of reconstruction samples, our framework improves over the Finetune baseline. (2) We find that different tuning strategies for the reconstruction hyperparameters can lead to further performance improvements. Previously, we adopted the naïve strategy when setting reconstruction-related hyperparameters due to the high computational overhead from the other strategies. Still, the naïve strategy outperforms the Finetune baseline

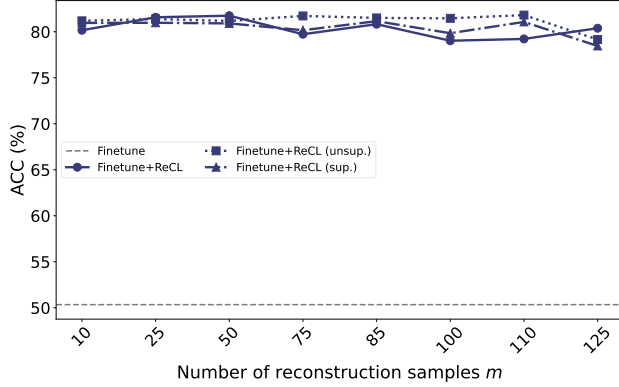


Figure 4. **Sensitivity to the number of reconstruction samples (scenario: CIL, SplitMNIST).** The performance gain increases for larger m , but already $m = 10$ outperforms *Finetune*.

by a large margin. (3) The supervised strategy outperforms the naïve one from above. This demonstrates that reconstructed data can be optimized by supervision with reference data. (4) The unsupervised tuning strategy for reconstruction strategy outperforms the *supervised* strategy. This is an interesting finding, as the unsupervised strategy does not need buffered reference data for hyperparameter tuning, which is beneficial in real-world applications.

Further results: We varied the number of reconstruction epochs from default $n_{\text{rec}} = 1000$ to study the sensitivity for MLPs trained on SplitMNIST (see Appendix H). We find that we can improve ACC up to 73.18 %, and already $n_{\text{rec}} = 500$ reconstruction epochs lead to improvements.

⇒ **Takeaway:** *Our ReCL slows down forgetting and improves the performance of existing CL baselines.*

6.2. Scenario DIL

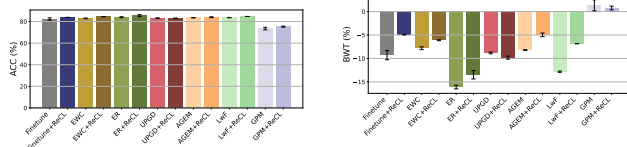


Figure 5. **ACC[↑] for DIL, SplitMNIST:** All methods benefit from our ReCL.

Main results: The results are in Figures 5 and 6 (with further results in Appendix F). We find: (1) When used standalone, our Finetune-ReCL slows down forgetting in comparison to the Finetune baseline by up to 1.92 % (ACC) and 47.15 % (BWT). (2) Our proposed ReCL is again highly effective: it slows down forgetting (higher BWT) and improves classification (higher ACC) for existing CL methods.

Further results: (1) The results for the sensitivity study are in Appendix F.1. We find that the performance is high

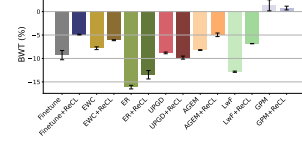


Figure 6. **BWT [↑] for DIL, SplitMNIST:** ReCL reduces forgetting for all methods.

Table 2. **Scenario DIL:** Results for training a MLP on SplitMNIST and CNN on SplitCIFAR10. Shown: average ACC[↑] and BWT[↑] over 5 random repetitions with varying order and init.

Method	SplitMNIST		SplitCIFAR10	
	ACC(±std)	BWT(±std)	ACC(±std)	BWT(±std)
Finetune	82.23 ± 1.09	-9.29 ± 1.36	62.59 ± 0.69	-10.57 ± 2.44
Finetune+ReCL	83.80 ± 0.06	-4.91 ± 0.13	63.87 ± 1.03	-10.27 ± 1.71
EWC	82.91 ± 0.29	-7.82 ± 0.31	64.09 ± 0.52	-9.40 ± 0.87
EWC+ReCL	84.48 ± 0.10	-6.11 ± 0.10	63.19 ± 0.31	-9.11 ± 1.13
ER	84.00 ± 0.38	-16.12 ± 0.50	64.11 ± 0.46	-9.95 ± 0.98
ER+ReCL	85.44 ± 0.91	-13.48 ± 1.12	64.08 ± 0.61	-8.43 ± 0.87
UPGD	83.19 ± 0.23	-8.82 ± 0.53	61.39 ± 0.51	-13.54 ± 1.16
UPGD+ReCL	82.95 ± 0.31	-9.82 ± 0.43	63.24 ± 0.41	-11.66 ± 0.80
AGEM	83.46 ± 0.11	-8.21 ± 0.19	61.97 ± 0.72	-13.19 ± 0.81
AGEM+ReCL	84.00 ± 0.39	-4.95 ± 0.96	62.03 ± 1.56	-12.54 ± 1.47
LwF	83.62 ± 0.13	-12.83 ± 0.15	65.66 ± 0.54	-4.17 ± 0.74
LwF+ReCL	84.67 ± 0.04	-6.84 ± 0.20	65.59 ± 0.45	-1.72 ± 0.43
GPM	73.48 ± 1.16	1.34 ± 1.01	60.64 ± 1.39	-4.56 ± 1.19
GPM+ReCL	75.29 ± 0.46	0.76 ± 0.92	61.98 ± 0.86	-1.91 ± 1.78

across all values, with the default 100 samples performing best. The naïve reconstruction strategy performs similar to the optimization strategies while adding considerably less computational overhead. (2) We further varied the number of reconstruction epochs (see Table 10) and find that 1 000 reconstruction epochs performs best, with no improvements from ablated settings. Overall, our ReCL framework leads to performance gains.

6.3. TinyImageNet

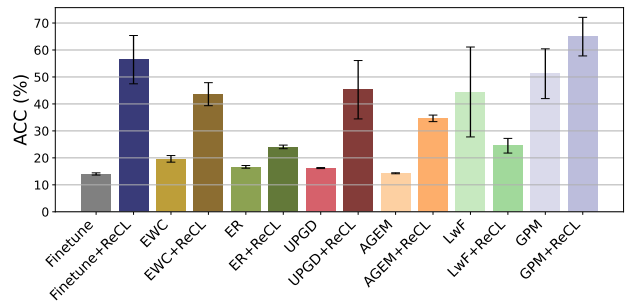


Figure 7. **ACC [↑] for DIL, TinyImageNet** All methods benefit from our ReCL. Used standalone, ReCL already is competitive to CL methods.

Main results: The results for SplitTinyImageNet are in Figure 7 (further results in Appendix G) and align with our previous findings. Notably, we find: (1) Used standalone, ReCL strongly improves the performance by 42 %p. (2) ReCL also improves existing CL methods in both the CIL and DIL scenarios.

⇒ **Takeaway:** *Our ReCL improves the performance of existing CL baselines on real-world data.*

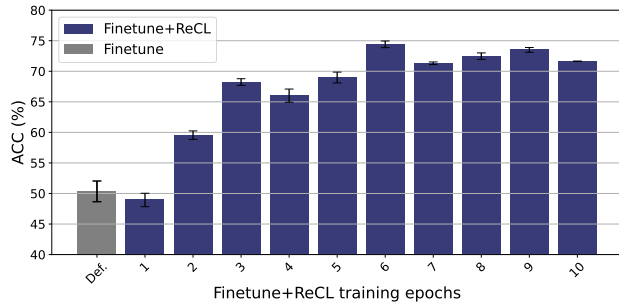


Figure 8. Ablation on train epochs for ReCL on **MNIST** in scenario **CIL**. Def. = default finetune performance without ReCL.

6.4. Further Insights

Can ReCL be used for online CL? For this, we evaluate ReCL in the challenging CIL scenario. Recall that in CIL, each task introduces novel classes. Additionally, in an online setup, each class’ samples are seen a limited number of times only, further increasing the difficulty. To simulate this, we deliberately vary the epochs from 1 to 10, thereby varying the strictness of the online CL. The results in Figure 8 show that strict online CL is not possible, but, already after two passes over the data, our ReCL improves the performance. Generally, more training epochs (i.e., more passes over the training data) increase the performance of ReCL.

Can ReCL slow down forgetting even for non-homogenous networks? For this, we use ReCL and now train AlexNet [28] and ResNet [20] in the DIL scenario. Both architectures are *not* homogenous neural networks because they use modules that introduce “jumps” into the propagation of hidden activations. AlexNet uses max-pooling, dropout [60] and bias vectors, and ResNet uses residual connections and batch normalization [23]. Both architectures thus violate the theoretical foundation of our CL framework. Nonetheless, we find that our ReCL is effective: it improves ACC by 4.77 % (AlexNet) and ~ 3 % (ResNet, Table 3; details in Appendix J). \Rightarrow **Takeaway:** *Our ReCL is also effective for non-homogenous network architectures where it can slow down forgetting successfully.*

Table 3. **Scenario DIL:** Results for using our framework with AlexNet [28] and ResNet18 [20], two *non*-homogenous neural networks violating the theoretical background of our framework. We nonetheless see improvements from using our ReCL.

Method	SplitCIFAR10	
	ACC	BWT
AlexNet	56.47	-31.63
AlexNet+ReCL	59.23	-28.25
ResNet	53.53	-28.17
ResNet+ReCL	55.16	-29.41

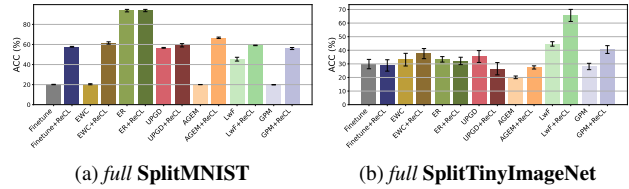


Figure 9. ACC for ReCL on *full* SplitMNIST and SplitTinyImageNet datasets.

Extended results for the full datasets. We now provide extended results for full datasets. For this, we select SplitMNIST and SplitTinyImageNet and use the entire training data. The results are visualized in Figure 9. Our observations align with our previous findings. We again find that our framework is highly effective, regardless of the size of the dataset. ReCL can improve the performance of methods that are known to underperform (e.g, EWC in CIL [63]) more than 40 %. At the same time, ReCL reduces the BWT by up to 122 %, sometimes even leading to *retrospective* performance improvements on old tasks. Detailed results are in Appendix I. \Rightarrow **Takeaway:** *Our ReCL can successfully slow down forgetting for large datasets.*

7. Conclusion

In this paper, we propose a novel framework for continual learning, termed ReCL (***R**econstruction for **C**ontinual **L**earning*), which slows down forgetting by using the neural network parameters as a built-in memory buffer. Different from existing approaches, our framework does not require separate generative networks or memory buffers. Instead, our ReCL framework offers a novel paradigm for dealing with forgetting by leveraging the implicit bias of convergence to margin maximization points. Through extensive experiments, we show that ReCL is compatible with (i) existing CL methods, (ii) different datasets, (iii) different dataset sizes, and (iv) different network architectures. Further, we also show the applicability of ReCL in challenging continual learning scenarios, namely class- and domain-incremental learning. Across all experiments, we observe consistent performance gains through our framework. Lastly, we expect our framework to be of practical value for real-world applications, where computational (e.g., sheer data size) or regulatory reasons only allow carrying over a limited amount of data from old tasks.

References

- [1] Takuya Akiba, Shotaro Sano, Toshihiko Yanase, Takeru Ohta, and Masanori Koyama. Optuna: A next-generation hyperparameter optimization framework. In *Proceedings of the 25th ACM SIGKDD international conference on knowledge discovery & data mining*, pages 2623–2631, 2019. 6, 3

- [2] Krizhevsky Alex. Learning multiple layers of features from tiny images. <https://www.cs.toronto.edu/kriz/learning-features-2009-TR.pdf>, 2009. 2, 5, 3
- [3] Ehsan Amid and Manfred KK Warmuth. Reparameterizing mirror descent as gradient descent. *Advances in Neural Information Processing Systems*, 33:8430–8439, 2020. 3, 1
- [4] Shahar Azulay, Edward Moroshko, Mor Shpigel Nacson, Blake E Woodworth, Nathan Srebro, Amir Globerson, and Daniel Soudry. On the implicit bias of initialization shape: Beyond infinitesimal mirror descent. In *International Conference on Machine Learning*, pages 468–477. PMLR, 2021. 3
- [5] Guy Blanc, Neha Gupta, Gregory Valiant, and Paul Valiant. Implicit regularization for deep neural networks driven by an ornstein-uhlenbeck like process. In *Conference on learning theory*, pages 483–513. PMLR, 2020. 3, 1
- [6] Léon Bottou. Online algorithms and stochastic approximations. *Online learning in neural networks*, 1998. 6, 4
- [7] Gavin Brown, Mark Bun, Vitaly Feldman, Adam Smith, and Kunal Talwar. When is memorization of irrelevant training data necessary for high-accuracy learning? In *Proceedings of the 53rd annual ACM SIGACT symposium on theory of computing*, pages 123–132, 2021. 3
- [8] Gon Buzaglo, Niv Haim, Gilad Yehudai, Gal Vardi, Yakir Oz, Yaniv Nikankin, and Michal Irani. Deconstructing data reconstruction: Multiclass, weight decay and general losses. *Advances in Neural Information Processing Systems*, 36, 2024. 3, 4, 5, 1, 2
- [9] Nicholas Carlini, Chang Liu, Úlfar Erlingsson, Jernej Kos, and Dawn Song. The secret sharer: Evaluating and testing unintended memorization in neural networks. In *28th USENIX security symposium (USENIX security 19)*, pages 267–284, 2019. 3
- [10] Arslan Chaudhry, Marc’Aurelio Ranzato, Marcus Rohrbach, and Mohamed Elhoseiny. Efficient lifelong learning with a gem. *arXiv preprint arXiv:1812.00420*, 2018. 2, 4
- [11] Arslan Chaudhry, Marcus Rohrbach, Mohamed Elhoseiny, Thalaiyasingam Ajanthan, Puneet K Dokania, Philip HS Torr, and Marc’Aurelio Ranzato. On tiny episodic memories in continual learning. *arXiv preprint arXiv:1902.10486*, 2019. 3
- [12] Andrea Cossu, Antonio Carta, Lucia Passaro, Vincenzo Lomonaco, Tinne Tuytelaars, and Davide Bacciu. Continual pre-training mitigates forgetting in language and vision. *Neural Networks*, 179:106492, 2024. 1
- [13] Alex Damian, Tengyu Ma, and Jason D Lee. Label noise sgd provably prefers flat global minimizers. *Advances in Neural Information Processing Systems*, 34:27449–27461, 2021. 3, 1
- [14] Danruo Deng, Guangyong Chen, Jianye Hao, Qiong Wang, and Pheng-Ann Heng. Flattening sharpness for dynamic gradient projection memory benefits continual learning. *Advances in Neural Information Processing Systems*, 34: 18710–18721, 2021. 1, 5, 3
- [15] Alexey Dosovitskiy. An image is worth 16x16 words: Transformers for image recognition at scale. *arXiv preprint arXiv:2010.11929*, 2020. 2
- [16] Mohamed Elsayed and A Rupam Mahmood. Addressing loss of plasticity and catastrophic forgetting in continual learning. *arXiv preprint arXiv:2404.00781*, 2024. 1, 2, 5, 3, 4
- [17] Suriya Gunasekar, Jason Lee, Daniel Soudry, and Nathan Srebro. Characterizing implicit bias in terms of optimization geometry. In *International Conference on Machine Learning*, pages 1832–1841. PMLR, 2018. 3, 1
- [18] Niv Haim, Gal Vardi, Gilad Yehudai, Ohad Shamir, and Michal Irani. Reconstructing training data from trained neural networks. *Advances in Neural Information Processing Systems*, 35:22911–22924, 2022. 3, 5, 1, 2, 4
- [19] Rujun Han, Xiang Ren, and Nanyun Peng. Econet: Effective continual pretraining of language models for event temporal reasoning. In *Proceedings of the 2021 Conference on Empirical Methods in Natural Language Processing*. Association for Computational Linguistics, 2021. 1
- [20] Kaiming He, Xiangyu Zhang, Shaoqing Ren, and Jian Sun. Deep residual learning for image recognition. In *Proceedings of the IEEE conference on computer vision and pattern recognition*, pages 770–778, 2016. 8, 2, 12
- [21] Y Hsu. Re-evaluating continual learning scenarios: A categorization and case for strong baselines. *arXiv preprint arXiv:1810.12488*, 2018. 2, 3
- [22] Julio Hurtado, Dario Salvati, Rudy Semola, Mattia Bosio, and Vincenzo Lomonaco. Continual learning for predictive maintenance: Overview and challenges. *Intelligent Systems with Applications*, 19:200251, 2023. 1
- [23] Sergey Ioffe. Batch normalization: Accelerating deep network training by reducing internal covariate shift. *arXiv preprint arXiv:1502.03167*, 2015. 8
- [24] Ziwei Ji and Matus Telgarsky. Directional convergence and alignment in deep learning. *Advances in Neural Information Processing Systems*, 33:17176–17186, 2020. 3, 4, 1, 2, 12
- [25] Haeyong Kang, Rusty John Lloyd Mina, Sultan Rizky Hikmawan Madjid, Jaehong Yoon, Mark Hasegawa-Johnson, Sung Ju Hwang, and Chang D Yoo. Forget-free continual learning with winning subnetworks. In *International Conference on Machine Learning*, pages 10734–10750. PMLR, 2022. 1
- [26] Zixuan Ke, Bing Liu, and Xingchang Huang. Continual learning of a mixed sequence of similar and dissimilar tasks. *Advances in neural information processing systems*, 33:18493–18504, 2020. 2
- [27] James Kirkpatrick, Razvan Pascanu, Neil Rabinowitz, Joel Veness, Guillaume Desjardins, Andrei A Rusu, Kieran Milan, John Quan, Tiago Ramalho, Agnieszka Grabska-Barwinska, et al. Overcoming catastrophic forgetting in neural networks. *Proceedings of the national academy of sciences*, 114(13):3521–3526, 2017. 1, 2, 5, 3
- [28] Alex Krizhevsky, Ilya Sutskever, and Geoffrey E Hinton. Imagenet classification with deep convolutional neural networks. *Advances in neural information processing systems*, 25, 2012. 8, 12
- [29] Ya Le and Xuan Yang. Tiny imagenet visual recognition challenge. *CS 231N*, 7(7):3, 2015. 2, 5, 3
- [30] Yann LeCun, Léon Bottou, Yoshua Bengio, and Patrick Haffner. Gradient-based learning applied to document recog-

- tion. *Proceedings of the IEEE*, 86(11):2278–2324, 1998. 2, 5, 3
- [31] Kibok Lee, Kimin Lee, Jinwoo Shin, and Honglak Lee. Overcoming catastrophic forgetting with unlabeled data in the wild. In *Proceedings of the IEEE/CVF International Conference on Computer Vision*, pages 312–321, 2019. 1
- [32] Zhizhong Li and Derek Hoiem. Learning without forgetting. *IEEE transactions on pattern analysis and machine intelligence*, 40(12):2935–2947, 2017. 1, 2, 5, 4
- [33] Zhiyuan Li, Tianhao Wang, and Sanjeev Arora. What happens after SGD reaches zero loss?—a mathematical framework. *arXiv preprint arXiv:2110.06914*, 2021. 3, 1
- [34] Noel Loo, Ramin Hasani, Mathias Lechner, Alexander Amini, and Daniela Rus. Understanding reconstruction attacks with the neural tangent kernel and dataset distillation. *arXiv preprint arXiv:2302.01428*, 2023. 1, 5
- [35] David Lopez-Paz and Marc’Aurelio Ranzato. Gradient episodic memory for continual learning. *Advances in neural information processing systems*, 30, 2017. 1, 2, 3, 5
- [36] Kaifeng Lyu and Jian Li. Gradient descent maximizes the margin of homogeneous neural networks. *arXiv preprint arXiv:1906.05890*, 2019. 3, 4, 1, 2, 12
- [37] Divyam Madaan, Jaehong Yoon, Yuanchun Li, Yunxin Liu, and Sung Ju Hwang. Representational continuity for unsupervised continual learning. In *10th International Conference on Learning Representations, ICLR 2022. International Conference on Learning Representations, ICLR, 2022*. 1
- [38] Mikel Malagon, Josu Ceberio, and Jose A. Lozano. Self-composing policies for scalable continual reinforcement learning. In *Proceedings of the 41st International Conference on Machine Learning*, pages 34432–34460. PMLR, 2024. 1
- [39] Arun Mallya and Svetlana Lazebnik. Packnet: Adding multiple tasks to a single network by iterative pruning. In *Proceedings of the IEEE conference on Computer Vision and Pattern Recognition*, pages 7765–7773, 2018. 1, 2
- [40] Michael McCloskey and Neal J Cohen. Catastrophic interference in connectionist networks: The sequential learning problem. In *Psychology of learning and motivation*, pages 109–165. Elsevier, 1989. 1, 2
- [41] Seyed Iman Mirzadeh, Mehrdad Farajtabar, Razvan Pascanu, and Hassan Ghasemzadeh. Understanding the role of training regimes in continual learning. *Advances in Neural Information Processing Systems*, 33:7308–7320, 2020. 1
- [42] Edward Moroshko, Blake E Woodworth, Suriya Gunasekar, Jason D Lee, Nati Srebro, and Daniel Soudry. Implicit bias in deep linear classification: Initialization scale vs training accuracy. *Advances in neural information processing systems*, 33:22182–22193, 2020. 3, 1
- [43] Martin Mundt, Iuliia Plushch, Sagnik Majumder, Yongwon Hong, and Visvanathan Ramesh. Unified probabilistic deep continual learning through generative replay and open set recognition. *Journal of Imaging*, 8(4):93, 2022. 1, 2
- [44] Mor Shpigel Nacson, Kavya Ravichandran, Nathan Srebro, and Daniel Soudry. Implicit bias of the step size in linear diagonal neural networks. In *International Conference on Machine Learning*, pages 16270–16295. PMLR, 2022. 3, 1
- [45] Mor Shpigel Nacson, Rotem Mulayoff, Greg Ongie, Tomer Michaeli, and Daniel Soudry. The implicit bias of minima stability in multivariate shallow relu networks. *arXiv preprint arXiv:2306.17499*, 2023. 3, 1
- [46] Behnam Neyshabur, Srinadh Bhojanapalli, David McAllester, and Nati Srebro. Exploring generalization in deep learning. *Advances in neural information processing systems*, 30, 2017. 3
- [47] Yakir Oz, Gilad Yehudai, Gal Vardi, Itai Antebi, Michal Irani, and Niv Haim. Reconstructing training data from real world models trained with transfer learning. *arXiv preprint arXiv:2407.15845*, 2024. 2
- [48] German I Parisi, Ronald Kemker, Jose L Part, Christopher Kanan, and Stefan Wermter. Continual lifelong learning with neural networks: A review. *Neural networks*, 113:54–71, 2019. 1
- [49] Alec Radford, Jong Wook Kim, Chris Hallacy, Aditya Ramesh, Gabriel Goh, Sandhini Agarwal, Girish Sastry, Amanda Askell, Pamela Mishkin, Jack Clark, et al. Learning transferable visual models from natural language supervision. In *International conference on machine learning*, pages 8748–8763. PMLR, 2021. 2
- [50] Jathushan Rajasegaran, Munawar Hayat, Salman H Khan, Fahad Shahbaz Khan, and Ling Shao. Random path selection for continual learning. *Advances in neural information processing systems*, 32, 2019. 5
- [51] Sylvestre-Alvise Rebuffi, Alexander Kolesnikov, Georg Sperl, and Christoph H Lampert. icarl: Incremental classifier and representation learning. In *Proceedings of the IEEE conference on Computer Vision and Pattern Recognition*, pages 2001–2010, 2017. 1, 2
- [52] David Rolnick, Arun Ahuja, Jonathan Schwarz, Timothy Lillicrap, and Gregory Wayne. Experience replay for continual learning. *Advances in neural information processing systems*, 32, 2019. 1, 2, 5, 3
- [53] Andrei A Rusu, Neil C Rabinowitz, Guillaume Desjardins, Hubert Soyer, James Kirkpatrick, Koray Kavukcuoglu, Razvan Pascanu, and Raia Hadsell. Progressive neural networks. *arXiv preprint arXiv:1606.04671*, 2016. 1, 2, 3
- [54] Gobinda Saha, Isha Garg, and Kaushik Roy. Gradient projection memory for continual learning. In *International Conference on Learning Representations*, 2021. 1, 2, 3, 5, 4
- [55] Joan Serra, Didac Suris, Marius Miron, and Alexandros Karatzoglou. Overcoming catastrophic forgetting with hard attention to the task. In *ICML*, 2018. 5, 3
- [56] Khadija Shaheen, Muhammad Abdullah Hanif, Osman Hasan, and Muhammad Shafique. Continual learning for real-world autonomous systems: Algorithms, challenges and frameworks. *Journal of Intelligent & Robotic Systems*, 105(1):9, 2022. 1
- [57] Yujun Shi, Kuangqi Zhou, Jian Liang, Zihang Jiang, Jia-ashi Feng, Philip HS Torr, Song Bai, and Vincent YF Tan. Mimicking the oracle: An initial phase decorrelation approach for class incremental learning. In *Proceedings of the IEEE/CVF conference on computer vision and pattern recognition*, pages 16722–16731, 2022. 1

- [58] Hanul Shin, Jung Kwon Lee, Jaehong Kim, and Jiwon Kim. Continual learning with deep generative replay. *Advances in neural information processing systems*, 30, 2017. [1](#), [2](#)
- [59] Jascha Sohl-Dickstein, Eric Weiss, Niru Maheswaranathan, and Surya Ganguli. Deep unsupervised learning using nonequilibrium thermodynamics. In *International conference on machine learning*, pages 2256–2265. PMLR, 2015. [2](#)
- [60] Nitish Srivastava, Geoffrey Hinton, Alex Krizhevsky, Ilya Sutskever, and Ruslan Salakhutdinov. Dropout: a simple way to prevent neural networks from overfitting. *The journal of machine learning research*, 15(1):1929–1958, 2014. [3](#), [8](#)
- [61] Sebastian Thrun and Tom M Mitchell. Lifelong robot learning. *Robotics and autonomous systems*, 15(1-2):25–46, 1995. [1](#)
- [62] Narek Tumanyan, Omer Bar-Tal, Shai Bagon, and Tali Dekel. Splicing vit features for semantic appearance transfer. In *Proceedings of the IEEE/CVF Conference on Computer Vision and Pattern Recognition*, pages 10748–10757, 2022. [2](#)
- [63] Gido M Van de Ven and Andreas S Tolias. Three scenarios for continual learning. *arXiv preprint arXiv:1904.07734*, 2019. [2](#), [8](#)
- [64] Gido M Van de Ven, Hava T Siegelmann, and Andreas S Tolias. Brain-inspired replay for continual learning with artificial neural networks. *Nature communications*, 2020. [2](#)
- [65] Gido M Van de Ven, Tinne Tuytelaars, and Andreas S Tolias. Three types of incremental learning. *Nature Machine Intelligence*, 4(12):1185–1197, 2022. [2](#), [3](#), [5](#)
- [66] Gal Vardi. On the implicit bias in deep-learning algorithms. *Communications of the ACM*, 66(6):86–93, 2023. [2](#)
- [67] Kerstin N Vokinger, Stefan Feuerriegel, and Aaron S Kesselheim. Continual learning in medical devices: Fda’s action plan and beyond. *The Lancet Digital Health*, 3(6):e337–e338, 2021. [1](#)
- [68] Bohan Wang, Qi Meng, Wei Chen, and Tie-Yan Liu. The implicit bias for adaptive optimization algorithms on homogeneous neural networks. In *International Conference on Machine Learning*, pages 10849–10858. PMLR, 2021. [3](#), [1](#)
- [69] Liyuan Wang, Kuo Yang, Chongxuan Li, Lanqing Hong, Zhenguo Li, and Jun Zhu. Ordisco: Effective and efficient usage of incremental unlabeled data for semi-supervised continual learning. In *Proceedings of the IEEE/CVF Conference on Computer Vision and Pattern Recognition*, pages 5383–5392, 2021. [1](#)
- [70] Liyuan Wang, Xingxing Zhang, Hang Su, and Jun Zhu. A comprehensive survey of continual learning: theory, method and application. *IEEE Transactions on Pattern Analysis and Machine Intelligence*, 2024. [1](#), [2](#)
- [71] Zhou Wang, Alan C Bovik, Hamid R Sheikh, and Eero P Simoncelli. Image quality assessment: from error visibility to structural similarity. *IEEE transactions on image processing*, 13(4):600–612, 2004. [5](#), [4](#)
- [72] Mitchell Wortsman, Vivek Ramanujan, Rosanne Liu, Aniruddha Kembhavi, Mohammad Rastegari, Jason Yosinski, and Ali Farhadi. Supermasks in superposition. *Advances in Neural Information Processing Systems*, 33:15173–15184, 2020. [1](#)
- [73] Tz-Ying Wu, Gurumurthy Swaminathan, Zhizhong Li, Avinash Ravichandran, Nuno Vasconcelos, Rahul Bhotika, and Stefano Soatto. Class-incremental learning with strong pre-trained models. In *Proceedings of the IEEE/CVF Conference on Computer Vision and Pattern Recognition*, pages 9601–9610, 2022. [1](#)
- [74] Enneng Yang, Li Shen, Zhenyi Wang, Tongliang Liu, and Guibing Guo. An efficient dataset condensation plugin and its application to continual learning. *Advances in Neural Information Processing Systems*, 36, 2023. [5](#)
- [75] Jaehong Yoon, Eunho Yang, Jeongtae Lee, and Sung Ju Hwang. Lifelong learning with dynamically expandable networks. In *International Conference on Learning Representations*, 2018. [2](#)
- [76] Jaehong Yoon, Saehoon Kim, Eunho Yang, and Sung Ju Hwang. Scalable and order-robust continual learning with additive parameter decomposition. In *Eighth International Conference on Learning Representations, ICLR 2020*. ICLR, 2020. [1](#), [3](#)
- [77] Runpeng Yu and Xinchao Wang. Generator born from classifier. *Advances in Neural Information Processing Systems*, 37, 2023. [4](#)
- [78] Friedemann Zenke, Ben Poole, and Surya Ganguli. Continual learning through synaptic intelligence. In *International conference on machine learning*, pages 3987–3995. PMLR, 2017. [2](#), [3](#), [5](#)
- [79] Chiyuan Zhang, Samy Bengio, Moritz Hardt, Benjamin Recht, and Oriol Vinyals. Understanding deep learning (still) requires rethinking generalization. *Communications of the ACM*, 64(3):107–115, 2021. [3](#)

Slowing Down Forgetting in Continual Learning

Supplementary Material

A. Extended Literature Review

Continual Learning: CL learning methods are often categorized into three categories, namely *memory-based*, *architecture-based*, and *regularization-based* [14, 54, 70].

Memory-based methods. Methods using memory-based techniques either maintain a (small) amount of old task’s data (or separate datasets) in a memory buffer or train generative models for old tasks. OrDisCo [69] uses a setup consisting of a generator, discriminator, and classifier to pseudo-label unlabelled data from a separate dataset and train these components together. iCarl [51] splits the feature and the classification parts of the network, and stores samples that are closest to the feature mean of a class. Variants of the gradient projection memory (GPM) approach [14, 54] store vectors describing the core gradient space in memory and guide update to be orthogonal to this space. In deep generative replay, Shin et al. [58] use a dual-network architecture consisting of an additional generative part that can be sampled for old tasks’ data.

Architecture-based methods. Methods based on architectural modifications allocate parts of a (growing) model to specific tasks. Progressive Neural Networks (PNN) [53] adds a separate network branch for new tasks and utilizes previous knowledge via lateral connections to previous tasks’ frozen branches, avoiding forgetting at the cost of growing network size. SupSup by Wortsman et al. [72] uses trained task-specific binary masks overlaid over a fixed random neural network to allocate parameters. The Winning Subnetworks (WSN) [25] approach follows a similar route, but allows training of the underlying neural network and restricts mask sizes. Finally, PackNet [39] prunes a task’s mask after training and then Finetunes the underlying weights while keeping parameters of previous tasks intact. APD [76] splits parameters into task-shared and task-specific parameters. They enforce sparsity on the task-specific parameters and retroactively update them to respond to changes in task-shared parameters.

Regularization-based methods. Methods in the regularization category use additional regularization terms in the loss function to restrict updates to important parameters. Examples here are elastic weight consolidation (EWC) [27], which uses the Fisher information matrix to assess parameter importance, and Learning without Forgetting (LwF) [32], which records the responses of the network to a new task’s data prior to training and tries to keep recorded and newly learned responses similar. Lee et al. [31] employ multiple distillation losses to distill the previous task’s model into a model combining the old and current tasks.

Additional categories. Beyond these three widely used categories, some taxonomies use five categories, adding the (i) *optimization* and (ii) *representation* approaches [70]. Methods belonging to the (i) **optimization** category manipulate the optimization process. The already introduced GPM approaches [14, 54] also fall into this category, as they modify gradient updates. Another method is StableSGD [41], which optimizes hyperparameters such as the learning rate in order to find flat minima which potentially “cover” all tasks. Methods belonging to the (ii) **representation** category focus on utilizing the representations learned during deep learning. Self-supervised learning and pre-training fall into this category, as they can provide a good initialization of neural networks for sequential downstream tasks [37, 57, 73]. Other methods explore continual pre-training, building on the fact that pre-training data might be collected incrementally [12, 19].

Implicit Bias and Data Reconstruction: Neural networks can generalize to unseen (test) data. This phenomenon is described as an *implicit bias* of neural network training, and it has been studied extensively [3–5, 13, 17, 33, 42, 44, 45, 68]. For a certain types of neural networks, described in Appendix B.1, the implicit bias causes network weights to converge to margin maximization points Ji and Telgarsky [24], Lyu and Li [36]. Haim et al. [18] show that under this condition, the entire training data can be recovered from pretrained binary classifiers. [34] utilized this for networks trained under the neural tangent kernel regime, and Buzaglo et al. [8] extend the underlying theory to multi-class networks and general loss functions.

B. Background on Dataset Reconstruction

In this section, we detail the background of the dataset reconstruction process, based on preliminary works [8, 18, 24, 36]. We start with the definition of *homogenous neural networks* and then give details on dataset reconstruction.

B.1. Homogenous Neural Networks

Homogenous networks are networks whose architectures satisfy the following condition [36]:

$$\forall c > 0 : \Phi(c\theta; x) = c^L \Phi(\theta; x) \text{ for all } \theta \text{ and } x, \quad (7)$$

if there is a $L > 0$. That is, scaling parameters θ is equal to scaling the network’s output $\Phi(\theta; x)$. Fully connected and convolutional neural networks with ReLu and without skip-connections and bias vectors satisfy this condition. However, popular models ResNet [20], ViT [15], or CLIP [49] models do not satisfy this condition since they contain modules (e.g., skip connections) that restrict the propagation of scaled weights’ intermediate outputs through the network. Oz et al. [47] show that in such cases, compute- and time-intensive workarounds relying on model inversion attacks [62] and diffusion models [59] could be applicable.

B.2. Dataset Reconstruction

Maximum margin points. To reconstruct the training data of past task, we build upon the implicit bias of gradient descent training [66]. For a homogenous neural network $\Phi(\theta, \cdot)$ trained under the gradient flow regime, Lyu and Li [36] show that the weights converge to the following maximum margin point

$$\min_{\theta} \frac{1}{2} \|\theta\|^2 \quad \text{s.t.} \quad \Phi_{y_i}(\theta; x_i) - \Phi_j(\theta; x_i) \geq 1 \quad \forall i \in [n], \forall j \in [C] \setminus \{y_i\}, \quad (8)$$

where $\Phi_j(\theta; x) \in \mathbb{R}$ is the output of the j -th neuron in the output layer for an input x_i and $[C]$ is the set of all classes (i.e., the label space). At such a point, the difference between the neuron activation of a sample’s true class, $\Phi_{y_i}(\theta; x_i)$, and all other neurons, $\Phi_j(\theta; x_i)$, is maximized.

Conditions. This convergence point is characterized by, among others, the existence of $\lambda_1, \dots, \lambda_m \in \mathbb{R}$ and the following *stationarity* and *feasibility* conditions [8]:

$$\theta - \sum_{i=1}^m \sum_{j \neq y_i}^c \lambda_{i,j} \nabla_{\theta} (\Phi_{y_i}(\theta; x_i) - \Phi_j(\theta; x_i)) = 0 \quad (9)$$

$$\forall i \in [n], \forall j \in [C] \setminus \{y_i\} : \lambda_{i,j} \geq 0 \quad (10)$$

These equations state that a (trained) neural network’s parameters θ can be approximated by linearly combining the λ -scaled derivatives on data points x_i . Keeping θ fixed, we

utilize this to optimize samples x_i and coefficients $\lambda_{i,j}$ using gradient descent. Note the following two things: (i) The corresponding labels y_i are chosen to match the number of output neurons of the pre-trained neural network⁵. We evenly split the number of classes among the samples to be reconstructed, but uneven splits are equally possible. (ii) The number of samples to reconstruct, m , generally is unknown. In this work, we consider it appropriate to maintain count of the number of samples of previous tasks. This could be achieved by, e.g., a small buffer which simply stores these counts. Determining the “correct” $m = n$ without prior knowledge is an open point and beyond the scope of this paper. As a starting point, we could imagine searching over a set of m and monitoring the behaviour of the reconstruction loss across trials.

Reconstruction loss: We reconstruct the old training data by optimizing randomly initialized data points x_i to closely resemble the old task’s data via the following combined reconstruction loss L_{full} [8]:

$$L_{\text{rec}}(x_1, \dots, x_m, \lambda_1, \dots, \lambda_m) = \left\| \theta - \sum_{i=1}^m \lambda_i \nabla_{\theta} \Phi(\theta; x_i) \right\|_2^2 + L_{\lambda} + L_{\text{prior}}, \quad (11)$$

where $\|\cdot\|_2^2$ denotes the squared L₂ norm (i.e., squared Euclidean distance). **Lambda loss:** The lambda loss L_{λ} constrains the coefficients of the linear combination via

$$L_{\lambda} = \sum_{i=1}^m \max \{-\lambda, -\lambda_{\min}\}, \quad (12)$$

where λ_{\min} is a hyperparameter.

Prior loss: The prior loss L_{prior} constrains the value range of the (reconstructed) images to lie within normalized range $[-1, 1]$.

Optimizing x_i and λ_i : We optimize the randomly initialized samples and coefficients via stochastic gradient descent. To backpropagate the gradients through Φ , we follow Haim et al. [18] and replace ReLU activations with a smooth ReLU function in the backwards pass only⁶.

B.3. Hyperparameters of the Reconstruction Process

The reconstruction process has several hyperparameters which influence reconstruction quality. First, the reconstructed samples x_i are initialized from a Gaussian distribution scaled by σ_x . In our in-training hyperparameter searches, we draw this parameter from a logarithmic

⁵E.g., if the network has three output neurons, then the class labels are $[1, 2, 3]$.

⁶In practice, we deepcopy Φ and on the copy replace ReLU activations with a smooth counterpart.

uniform distribution between $[10^{-5}, 1]$. The x_i are optimized gradient descent, with a learning rate log-uniform in $[10^{-5}, 1]$. For the separately-optimized coefficients λ_i , the learning rate is drawn from the same range. The λ_{\min} from Equation (3) is drawn log-uniform from $[0.01, 0.5]$. To optimize the hyperparameters in the *(un-)supervised* strategies detailed in Section 4.3, we run $n_{\text{trials}} = 100$ search trials using Bayesian search via Optuna [1]. As default, we use $n_{\text{rec}} = 1000$ reconstruction epochs at each trial.

C. Dataset Details

In this section, we give details about the three datasets used. All datasets are commonly used in previous works, [e.g., 14, 16, 27, 55, 65]. Below, we provide information about each of them.

MNIST: The MNIST [30] dataset contains 60 000 black-and-white 28x28 training images evenly split across 10 classes. An additional 10 000 samples are used for testing. The images show hand-written digits.

CIFAR10: The CIFAR10 [2] dataset contains 60 000 32x32 colour images evenly split across 10 classes. 50 000 samples are reserved for training and 10 000 samples for testing. This dataset depicts animals and vehicles.

TinyImagenet: The TinyImageNet [29] dataset contains 100 000 64x64 colour images from 200 classes. Note that test labels are unavailable. We thus follow [14] to create the training and testing splits. Further, we use a 40-class, two-task subset, with each task having 20 classes.

Pre-processing: We normalize the data by removing the training-data mean from each dataset.

Dataset Splitting: We split the datasets into $n_{\text{tasks}} = 5$ (value depending on the experiment) tasks by splitting the class labels without overlap. In the domain incremental learning (DIL) scenario, we dynamically re-label the classes to begin at zero. This is done to compute the cross-entropy loss of, e.g. classes [5, 6, 7, 8], on a model with an output layer of size four (which would expect labels [1, 2, 3, 4]).

D. Implementation details

In this section, we provide details about our implementation and the CL methods that we combine ReCL with.

D.1. Models

We train 4-layer multi-layer perceptron (MLP) and convolutional neural network (CNN) models. The MLP architecture is structured as D -1 000-1 000- C , where D is the (flattened) image input and C is the number of classes. The CNN architecture roughly follows [14]. It uses two convolution layers with 160 kernels of size 3, leading to $\text{CONV}(k=3, ch=160)$ - $\text{CONV}(k=3, ch=160)$ -640-320- C . Following the homogenous network constraint from Section 2 we use no bias vectors except for the first layer, whose weights are scaled by 10^{-4} . Note that for both network types, the number of neurons C in the final classification layer might be expanded over the course of incremental training.

D.2. Baseline Details

We implemented our *Reconstruction for Continual Learning* (ReCL) framework and the CL baselines in PyTorch. For this, we carefully considered available reference (UPGD [16], <https://github.com/mohmdelsayed/upgd>) and community implementations (EWC [27], <https://github.com/moskomule/ewc.pytorch>). We obtained written permission by the respective code maintainers. The same applies to the base code for the dataset reconstruction, which we derived from <https://github.com/gonbuzaglo/decoreco>.

Elastic weight consolidation:: Elastic weight consolidation (EWC) [27] is a regularization-based strategy that uses the Fisher Information Matrix to measure the importance of neural network parameters for a task. Based on the idea that the solution for a (new) task can be found in the neighbourhood of the current weights, it constrains parameters to stay close to their old value by adding the difference as a quadratic penalty. We refer to Kirkpatrick et al. [27] for details.

In both CL scenarios, we compute parameter importance after training on task τ from $\mathcal{D}_{\tau}^{\text{tr}}$. In the CIL scenario, which expands the output layer, we only constrain those values that existed before the expansion (i.e., the penalty for changing newly added parameters is zero).

Experience replay: Experience replay (ER) [11, 52] is a memory-based strategy that stores a small subset of the old tasks’ training data in a memory buffer. It then replays this buffered data in training on task τ . ER has originally been proposed in reinforcement learning to help an agent learn from previous experience.

In all experiments, we set a default buffer size of 10 % by selecting a random subset of a task’s training data for storage in memory. We do not employ any optimization

strategies (such as choosing the hardest or most informative data points) when adding to or drawing from the memory buffer.

Utility-perturbed gradient descent: Utility-perturbed gradient descent (UPGD) [16] is a regularization-based and optimization-based strategy based on the idea of pruning (un-)important parameters. It directly modifies a parameter’s gradient as follows. (i) First, it computes the performance difference between the network as-is and with the parameter set to zero. However, this is computationally prohibitive as it would require a separate forward pass for each parameter. UPGD therefore approximates the true utility of a parameter using Taylor approximation. (ii) Second, it scales per-parameter gradients based on their utility. For more useful (=important) parameters, the gradient update size is reduced, while for non-useful parameters it is not modified. Crucially, UPGD adds Gaussian noise to the gradient. We refer to Elsayed and Mahmood [16] for details.

Average-gradient episodic memory: AGEM [10] is a replay- and optimization-based strategy. It stores a small number of samples (called *experiences*) in memory. During training on the current task, AGEM uses the stored old samples as an additional loss component, allowing that the average loss over all previous tasks does not increase.

Learning without Forgetting: Learning without Forgetting (LwF) [32] is an optimization-based strategy that, at the beginning of each task, stores reference outputs of the model for the current task’s data. During training, the strategy penalizes changes to the network that cause the output deviate too strongly from the reference outputs. It thus searches for parameters that encode the current information and simultaneously avoid catastrophic inference.

Gradient projection memory: Gradient projection memory (GPM) [54] is a replay- and optimization-based strategy. GPM computes the bases of the weight space spanned by the model’s parameters, and updates the set of bases at each new task. Gradients are then projected to be orthogonal to the current space.

Combination with ReCL: We combine ReCL with the above listed CL baseline methods by adding it on top. For this, no modifications are necessary as the data reconstruction is independent. This highlights the flexibility of our framework.

D.3. Hyperparameter search ranges

We optimized the hyperparameters of each CL method (EWC, UPGD, ER) and our baselines separately over 100 trials on a held-out validation dataset (a subset of the training data). Optimized hyperparameters and their search ranges are given in Table 4.

D.4. Training Details

All networks are trained with stochastic gradient descent (SGD) [6] with a batch size of 64. We use the cross-entropy loss based on logits (i.e., no activation on ϕ_h , following Appendix B.1). We repeat each experiment 5 times, each time with a different seed.

In preliminary experiments, we followed previous works [8, 18] and used full-batch gradient descent, with the batch size chosen to fit the entire training data. However, we found that (i) large batch sizes are detrimental for both the “normally” trained models and models trained with reconstructed data, and (ii) data reconstruction also works with smaller batch sizes (e.g. 64). We thus used mini-batch SGD as the optimizer.

D.5. Computing the Similarity Between Reconstructed and Reference Samples

In this section, we give details on how we compute the similarity between reconstructed and reference samples used in the proposed *supervised* strategy (see Section 4.3). We also suggest two possible improvements that could be explored in future works.

For computing image similarity, we closely follow [18] in performing the following two steps.

Step 1: Distance calculation. For each reference sample x_{ref} , we compute the following distance to all reconstructed samples x_{recon} :

$$d(x_{\text{ref}}, x_{\text{recon}}) = \|\hat{x}_{\text{ref}} - \hat{x}_{\text{recon}}\|_2^2, \quad (13)$$

where \hat{x}_{ref} is obtained by reducing from x_{ref} the mean of all reference samples and then dividing it by the standard deviation of all reference samples. The same steps are respectively applied to obtain \hat{x}_{recon} . We select for each training sample its closest reconstructed neighbour.

Step 2: Sample creation. (i) We re-add the training set mean (note that our data is normalized to $[-1, 1]$ by reducing the training mean from all data points) to reconstructed samples \hat{x}_{recon} and reference samples x_{ref} . (ii) We then stretch the x_{ref} to $[0, 1]$ by scaling according to the minimum and maximum value. (iii) Lastly, we compute the SSIM [71] between the pair.

Possible improvements. We see the following possible ways to improve the reconstruction process. (i) We remark that assessing image similarity (or aesthetics of generated images) is a subjective and open process in research. However, we think that future work could improve our ReCL by filtering for reconstructed samples that fill certain *real data-like* criteria. Previous works by [18] used a SSIM score of above 0.4 as threshold, but other thresholds and similarity metrics are possible.

(ii) We currently do not enforce reconstructed samples to be unique. As a result, two reconstructed samples might

Table 4. Hyperparameter search space. The search ranges for the EWC and UPGD parameters are from [16]. The hyperparameter search is conducted separately for each CL scenario, architecture, and dataset over 100 trials. “For” denotes the methods for which we optimized the listed hyperparameters.

Parameter	Search Space	For
Learning rate	0.0001 to 0.1 (log uniform)	All
Train epochs	10 to 100	All
EWC- λ	{10, 100, 500, 1000, 2500, 5000, 10000}	EWC
Replay fine-tuning epochs	1 to 10	ER
Patterns per experience	{1, 10, 25, 50}	AGEM
GPM thresholds	{0.9, 0.99, 0.999}	GPM
LwF- λ	{0.1, 0.5, 1, 2, 4, 8, 10}	LwF
LwF temperature	{0.5, 1, 2, 4}	LwF
UPGD- β	0.9 to 0.9999	UPGD
UPGD- σ	0.0001 to 0.01	UPGD
Extraction epochs	{100, 500, 1000}	ReCL
Extraction learning rate	0.0001 to 1.0 (log uniform)	ReCL
Extraction lambda learning rate	0.0001 to 1.0 (log uniform)	ReCL
Extraction min lambda	0.01 to 0.5 (log uniform)	ReCL
Extraction model ReLU alpha	10 to 500	ReCL
Extraction init scale	0.000001 to 0.1 (log uniform)	ReCL
Hyperparameter num trials	{10, 25, 50, 100, 150}	ReCL

provide the same (non-)new information to the machine learning model. Here, combining close reconstructed samples by, *e.g.*, naïve overlaying or more sophisticated dataset distillation techniques [cf. 34, 74]. These methods are applicable post-reconstruction. Alternatively one could enforce pairwise dissimilarity during minimization of Equation (6).

E. Result for CIL

In this section, we provide extended results for the experiments reported in Section 6.1. Table 9 shows ACC and BWT for a MLP trained with varying reconstructed samples on SplitMNIST.

E.1. Sensitivity Analysis for the CIL scenario

In this section, we give details on the sensitivity analysis of our ReCL to the number of reconstruction samples m . Results are in Table 5. ReCL is already competitive when merely reconstructing $m = 10$ training samples.

Table 5. **Scenario CIL:** Classification performance with varying number of reconstruction samples m . Shown: average ACC[\uparrow] and BWT[\uparrow] over 5 random repetitions with varying task order and initialization.

m	Method	ACC(\pm std)	BWT(\pm std)
10	Finetune+ReCL	49.36 \pm 4.13	-51.02 \pm 5.63
	Finetune+ReCL (unsup.)	61.92 \pm 3.73	-36.16 \pm 8.25
	Finetune+ReCL (sup.)	54.34 \pm 5.66	-42.14 \pm 12.08
25	Finetune+ReCL	58.16 \pm 0.34	-38.58 \pm 1.28
	Finetune+ReCL (unsup.)	60.54 \pm 2.62	-38.07 \pm 5.58
	Finetune+ReCL (sup.)	56.32 \pm 3.83	-46.04 \pm 4.88
50	Finetune+ReCL	63.83 \pm 3.69	-31.91 \pm 5.44
	Finetune+ReCL (unsup.)	61.39 \pm 7.28	-34.13 \pm 9.13
	Finetune+ReCL (sup.)	59.37 \pm 5.50	-39.15 \pm 7.42
75	Finetune+ReCL	73.41 \pm 1.38	-20.67 \pm 1.58
	Finetune+ReCL (unsup.)	64.24 \pm 2.02	-25.03 \pm 10.42
	Finetune+ReCL (sup.)	67.07 \pm 4.09	-24.26 \pm 10.61
85	Finetune+ReCL	67.30 \pm 3.07	-28.25 \pm 4.42
	Finetune+ReCL (unsup.)	67.13 \pm 3.11	-16.36 \pm 7.76
	Finetune+ReCL (sup.)	64.84 \pm 5.88	-29.69 \pm 9.93
100	Finetune+ReCL	71.76 \pm 1.88	-21.82 \pm 1.34
	Finetune+ReCL (unsup.)	66.99 \pm 3.05	-20.64 \pm 9.20
	Finetune+ReCL (sup.)	67.45 \pm 3.17	-23.49 \pm 7.81
110	Finetune+ReCL	70.18 \pm 0.84	-22.92 \pm 0.84
	Finetune+ReCL (unsup.)	66.66 \pm 2.48	-13.55 \pm 2.78
	Finetune+ReCL (sup.)	69.99 \pm 0.72	-14.51 \pm 5.44
125	Finetune+ReCL	65.08 \pm 1.18	-29.24 \pm 3.22
	Finetune+ReCL (unsup.)	62.11 \pm 5.51	-13.87 \pm 6.15
	Finetune+ReCL (sup.)	67.84 \pm 4.59	-18.87 \pm 8.19

E.2. CIFAR10 visualization

Below, we provide visualizations for ReCL with state-of-the-art CL methods on the CIFAR10 dataset. Tabular results are in Table 1 in the main text, Section 6.1.

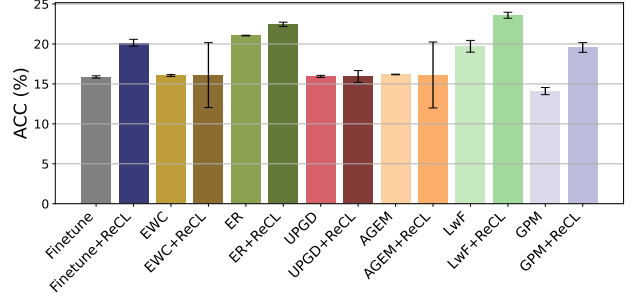


Figure 10. **ACC [\uparrow] for CIL, SplitCIFAR10.** All methods benefit from our ReCL. Used standalone, ReCL already is competitive to CL methods.

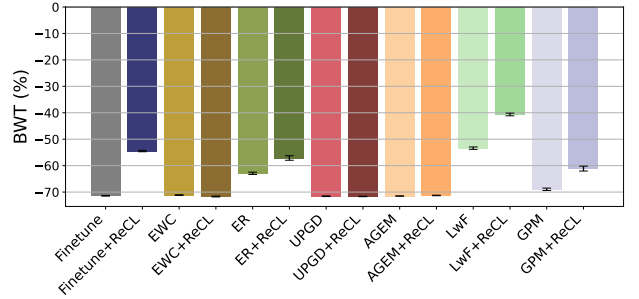


Figure 11. **BWT [\uparrow] for CIL, SplitCIFAR10.** ReCL strongly reduces forgetting for all methods and is competitive when used standalone.

F. Results for DIL

In this section, we provide the full results for the experiments reported in Section 6.2. Table 9 shows ACC and BWT for a MLP trained with varying reconstructed samples on SplitMNIST.

F.1. Sensitivity Analysis DIL

In this section, we give details on the sensitivity analysis of our ReCL to the number of reconstruction samples m in the DIL scenario. The results are in Table 6. ReCL is already competitive when merely reconstructing $m = 10$ samples while adding minimal computational overhead.

Table 6. **Scenario DIL:** Classification performance with varying number of reconstruction samples m . Shown: average ACC[\uparrow] and BWT[\uparrow] over 5 random repetitions with varying task order and initialization.

m	Method	ACC(\pm std)	BWT(\pm std)
10	Finetune+ReCL	80.17 ± 0.13	-9.64 ± 2.25
	Finetune+ReCL (unsup.)	81.19 ± 0.71	-8.35 ± 1.01
	Finetune+ReCL (sup.)	80.99 ± 0.76	-10.64 ± 2.37
25	Finetune+ReCL	81.58 ± 0.31	-7.74 ± 2.20
	Finetune+ReCL (unsup.)	81.39 ± 0.23	-7.67 ± 3.79
	Finetune+ReCL (sup.)	80.98 ± 0.81	-9.48 ± 2.95
50	Finetune+ReCL	81.75 ± 0.40	-7.64 ± 1.26
	Finetune+ReCL (unsup.)	81.18 ± 0.25	-7.91 ± 0.55
	Finetune+ReCL (sup.)	80.91 ± 0.85	-10.23 ± 2.57
75	Finetune+ReCL	79.74 ± 1.46	-17.87 ± 1.81
	Finetune+ReCL (unsup.)	81.72 ± 0.55	-4.55 ± 0.93
	Finetune+ReCL (sup.)	81.17 ± 0.71	-9.42 ± 1.48
85	Finetune+ReCL	80.83 ± 0.08	-10.33 ± 2.69
	Finetune+ReCL (unsup.)	81.51 ± 0.39	-5.29 ± 1.34
	Finetune+ReCL (sup.)	81.19 ± 0.77	-9.56 ± 2.61
100	Finetune+ReCL	83.80 ± 0.06	-4.91 ± 0.13
	Finetune+ReCL (unsup.)	81.36 ± 0.64	-5.69 ± 2.39
	Finetune+ReCL (sup.)	80.84 ± 0.63	-10.33 ± 2.66
110	Finetune+ReCL	79.22 ± 2.24	-20.02 ± 2.62
	Finetune+ReCL (unsup.)	81.82 ± 0.17	-8.10 ± 2.76
	Finetune+ReCL (sup.)	81.07 ± 0.50	-8.79 ± 0.42
125	Finetune+ReCL	80.39 ± 2.44	-17.97 ± 3.20
	Finetune+ReCL (unsup.)	81.35 ± 0.32	-6.18 ± 1.47
	Finetune+ReCL (sup.)	80.82 ± 0.62	-10.79 ± 2.01

F.2. CIFAR10 visualization

We here provide visualizations for ReCL with state-of-the-art CL methods on the CIFAR10 dataset. Tabular results are in Table 2 in the main text, Section 6.2.

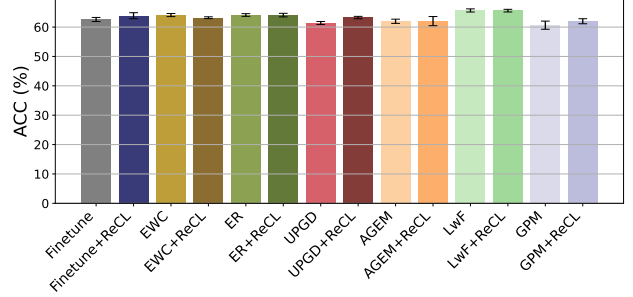


Figure 12. **ACC [\uparrow] for DIL, SplitCIFAR10.** All methods benefit from our ReCL. Used standalone, ReCL already is competitive to CL methods.

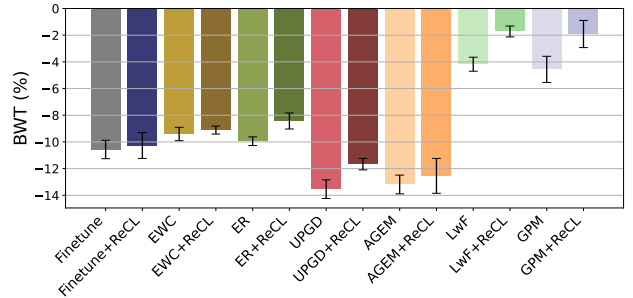


Figure 13. **BWT [\uparrow] for DIL, SplitCIFAR10.** ReCL strongly reduces forgetting for all methods and is competitive when used standalone.

G. Results on TinyImageNet

In this section, we provide the full results for the experiments reported in Section 6.3. Tables 7 and 8 show the tabular results for Figures 14 and 15.

Table 7. **Scenario CIL:** Results on SplitTinyImageNet. Shown: average ACC[↑] and BWT[↑] over 5 random repetitions with varying order and init.

Approach	ACC(\pm std)	BWT(\pm std)
Finetune	33.58 ± 8.40	-47.50 ± 23.52
Finetune+ReCL	39.68 ± 4.56	-35.00 ± 0.59
ewc	37.28 ± 5.49	-79.20 ± 7.07
ewc+ReCL	38.93 ± 2.89	-33.77 ± 2.68
er	12.57 ± 0.15	-24.20 ± 0.71
er+ReCL	30.38 ± 0.84	-50.57 ± 1.25
upgd	44.93 ± 0.94	-88.73 ± 3.18
upgd+ReCL	16.05 ± 1.13	-36.73 ± 4.53
agem	33.28 ± 2.03	-66.93 ± 7.33
agem+ReCL	24.62 ± 1.55	-48.47 ± 0.88
lwf	29.53 ± 2.86	-17.80 ± 6.76
lwf+ReCL	32.53 ± 2.40	-17.80 ± 4.85
gpm	44.82 ± 1.20	-87.17 ± 2.44
gpm+ReCL	47.48 ± 3.56	-21.03 ± 10.72

Table 8. **Scenario DIL:** Results on SplitTinyImageNet. Shown: average ACC[↑] and BWT[↑] over 5 random repetitions with varying order and init.

Approach	ACC(\pm std)	BWT(\pm std)
Finetune	14.03 ± 0.41	-19.90 ± 3.05
Finetune+ReCL	56.42 ± 8.96	-33.13 ± 1.92
EWC	19.63 ± 1.23	-17.07 ± 0.66
EWC+ReCL	43.62 ± 4.27	-31.27 ± 2.49
ER	16.67 ± 0.50	-11.73 ± 0.90
ER+ReCL	24.07 ± 0.67	-14.67 ± 0.21
UPGD	16.22 ± 0.19	-17.13 ± 0.21
UPGD+ReCL	45.27 ± 10.82	-49.93 ± 6.08
AGEM	14.28 ± 0.18	-17.60 ± 0.14
AGEM+ReCL	34.65 ± 1.21	-23.87 ± 0.68
LwF	44.43 ± 16.67	-7.07 ± 1.93
LwF+ReCL	24.50 ± 2.72	-16.70 ± 0.24
GPM	51.20 ± 9.22	-27.27 ± 2.47
GPM+ReCL	64.95 ± 7.15	-15.90 ± 1.79

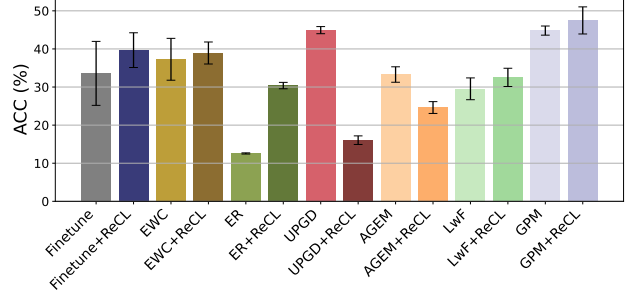


Figure 14. **ACC [↑] for CIL, SplitTinyImageNet.** All methods benefit from our ReCL. Used standalone, ReCL already is competitive to CL methods.

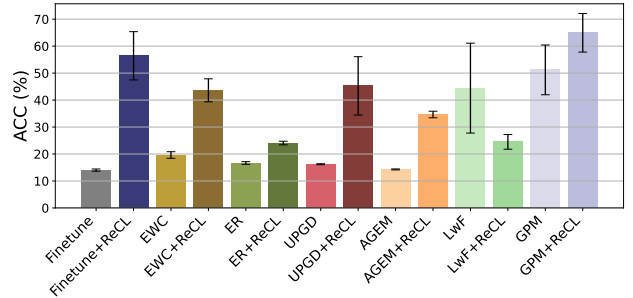


Figure 15. **ACC [↑] for DIL, SplitTinyImageNet.** All methods benefit from our ReCL. Used standalone, ReCL already is competitive to CL methods.

H. Varying the number of reconstruction epochs

Here, we present results when varying the number of reconstruction epochs in the CIL and DIL scenario. We train a MLP on the SplitMNIST dataset and vary n_{rec} as [500, 1000, 2500, 5000, 10000].

The results are in Tables 9 and 10. We observe that more reconstruction epochs are mostly beneficial in the CIL scenario, whereas they have little effect on the DIL scenario.

Table 9. **Scenario CIL:** Results for varying reconstruction epochs n_{rec} (default: 1000). Shown: average ACC[↑], BWT[↑], and runtime over 5 random repetitions with varying task order and initialization.

m	Method	ACC(\pm std)	BWT(\pm std)
500	Finetune+ReCL	70.04 \pm 3.06	-23.38 \pm 7.29
1000	Finetune+ReCL	73.18 \pm 0.09	-14.51 \pm 1.64
2500	Finetune+ReCL	68.80 \pm 1.25	-22.36 \pm 4.28
5000	Finetune+ReCL	66.94 \pm 1.19	-22.69 \pm 10.05
10000	Finetune+ReCL	67.87 \pm 3.65	-23.93 \pm 8.60

Table 10. **Scenario DIL:** Results for varying reconstruction epochs n_{rec} (default: 1000). Shown: average ACC[↑], BWT[↑], and runtime over 5 random repetitions with varying task order and initialization.

m	Method	ACC(\pm std)	BWT(\pm std)
500	Finetune+ReCL	73.84 \pm 3.96	4.20 \pm 3.38
1000	Finetune+ReCL	83.80 \pm 0.06	-4.91 \pm 0.13
2500	Finetune+ReCL	78.05 \pm 0.46	-1.43 \pm 3.39
5000	Finetune+ReCL	73.42 \pm 6.20	0.82 \pm 4.85
10000	Finetune+ReCL	74.47 \pm 5.95	0.08 \pm 4.16

I. Extended results for large-scale datasets

In this section, we present extended results for applying ReCL to large-scale (i.e., full) datasets. For this, we select SplitMNIST and SplitTinyImageNet and use the entire training data. We use the same architectures (Appendix D) as before, but set the number of reconstruction samples to 1000 and 600 for SplitMNIST and SplitTinyImageNet, respectively. Again, we optimize the hyperparameters for each experiment separately over the grid given in Appendix D and Tab. 4. The results are in Table 11 to Table 14.

Our findings align with our previous observations, and ReCL also slows down forgetting for larger datasets. Note how ReCL can even lead to retrospective performance improvements on past tasks, as the *positive* BWT for method LwF indicates.

Table 11. **Scenario CIL: Results on full SplitMNIST.** Shown: average ACC[↑] and BWT[↑] over 5 random repetitions with varying task order and init.

Approach	ACC(\pm std)	BWT(\pm std)
Finetune	20.08 \pm 0.21	-99.45 \pm 0.40
Finetune+ReCL	57.74 \pm 0.36	-50.49 \pm 3.62
EWC	20.35 \pm 0.53	-99.05 \pm 0.81
EWC+ReCL	61.50 \pm 1.16	-44.54 \pm 2.64
ER	93.73 \pm 1.24	-6.98 \pm 0.38
ER+ReCL	93.83 \pm 1.14	-6.55 \pm 0.54
UPGD	56.65 \pm 0.40	-45.52 \pm 1.52
UPGD+ReCL	59.20 \pm 1.65	-47.61 \pm 7.49
AGEM	20.01 \pm 0.11	-99.64 \pm 0.14
AGEM+ReCL	66.68 \pm 0.68	-38.60 \pm 4.39
LwF	45.35 \pm 1.90	-39.55 \pm 6.29
LwF+ReCL	59.08 \pm 0.27	4.58 \pm 2.33
GPM	19.87 \pm 0.23	-98.47 \pm 0.78
GPM+ReCL	55.97 \pm 1.03	-51.77 \pm 7.20

Table 12. **Scenario CIL: Results on full SplitTinyImageNet.** Shown: average ACC[↑] and BWT[↑] over 5 random repetitions with varying task order and init.

Approach	ACC(\pm std)	BWT(\pm std)
Finetune	29.85 \pm 3.44	-51.23 \pm 4.78
Finetune+ReCL	28.85 \pm 4.19	-46.70 \pm 3.41
EWC	33.10 \pm 4.65	-60.70 \pm 1.89
EWC+ReCL	37.55 \pm 3.72	-50.60 \pm 2.87
ER	33.33 \pm 2.01	-58.23 \pm 4.45
ER+ReCL	32.17 \pm 2.71	-45.47 \pm 3.76
UPGD	35.42 \pm 4.36	-69.10 \pm 9.41
UPGD+ReCL	26.45 \pm 4.51	-47.80 \pm 1.63
AGEM	20.10 \pm 0.97	-48.07 \pm 1.59
AGEM+ReCL	27.38 \pm 1.16	-49.43 \pm 0.75
LwF	44.68 \pm 1.64	-26.43 \pm 4.01
LwF+ReCL	65.63 \pm 4.43	-19.10 \pm 4.09
GPM	28.08 \pm 2.34	-67.17 \pm 6.18
GPM+ReCL	40.55 \pm 2.87	-49.83 \pm 6.96

Table 13. **Scenario DIL: Results on full SplitMNIST.** Shown: average ACC[↑] and BWT[↑] over 5 random repetitions with varying task order and init.

Approach	ACC(\pm std)	BWT(\pm std)
Finetune	79.26 \pm 1.01	-16.78 \pm 3.03
Finetune+ReCL	73.59 \pm 6.88	-32.44 \pm 8.03
EWC	74.79 \pm 7.76	-30.90 \pm 9.23
EWC+ReCL	76.49 \pm 0.96	-22.73 \pm 1.67
ER	96.85 \pm 0.15	-3.19 \pm 0.18
ER+ReCL	96.44 \pm 0.33	-3.62 \pm 0.32
UPGD	76.94 \pm 0.73	-21.62 \pm 1.96
UPGD+ReCL	78.99 \pm 0.89	-17.74 \pm 2.80
AGEM	73.80 \pm 6.45	-32.30 \pm 8.25
AGEM+ReCL	77.18 \pm 6.23	-27.85 \pm 7.26
LwF	83.27 \pm 1.73	-1.17 \pm 1.64
LwF+ReCL	82.58 \pm 2.36	8.58 \pm 0.95
GPM	66.56 \pm 3.08	-0.73 \pm 0.90
GPM+ReCL	76.28 \pm 4.25	-28.22 \pm 4.54

Table 14. **Scenario DIL: Results on *full* SplitTinyImageNet.**
Shown: average ACC[↑] and BWT[↑] over 5 random repetitions
with varying task order and init.

Approach	ACC(\pm std)	BWT(\pm std)
Finetune	54.80 ± 8.80	-40.17 ± 2.23
Finetune+ReCL	23.77 ± 4.78	-12.20 ± 4.74
EWC	45.68 ± 9.66	-40.30 ± 3.77
EWC+ReCL	25.78 ± 2.10	-15.30 ± 1.06
ER	44.45 ± 12.41	-32.53 ± 6.89
ER+ReCL	44.72 ± 1.90	-18.40 ± 1.00
UPGD	47.37 ± 4.52	-52.67 ± 2.41
UPGD+ReCL	30.38 ± 1.53	-29.77 ± 2.53
AGEM	41.62 ± 7.71	-48.03 ± 2.73
AGEM+ReCL	44.08 ± 2.36	-35.37 ± 0.97
LwF	54.08 ± 4.61	-18.50 ± 0.41
LwF+ReCL	63.22 ± 20.13	-12.77 ± 3.76
GPM	57.05 ± 14.09	-36.53 ± 1.52
GPM+ReCL	54.32 ± 2.54	-12.67 ± 5.00

J. ReCL slows down forgetting beyond theoretical limitations

In the main text, we focus on MLPs and CNNs, which generally conform to the definition of homogenous neural networks (cf. Appendix B.1). These type of neural networks converge to margin maximization points Ji and Telgarsky [24], Lyu and Li [36]. To slow down forgetting in CL, our ReCL builds on these convergence points, as they allow the (unsupervised) reconstruction of old training data. Interestingly, ReCL can also slow down forgetting for networks that are explicitly *not* homogenous, such as AlexNet [28] and ResNet [20].

To demonstrate this, we perform the following additional experiment. We optimize the training hyperparameters of AlexNet and Resnet in the DIL scenario, on the SplitCIFAR10 dataset, following the same search procedure as for the other networks (Section 5 and Appendix D). That is, over 100 hyperparameter trials, we optimize the learning rate and training epochs over the grid details in Table 4. We then train AlexNet and ResNet with (+ReCL) and without our framework.

Our results are in Table 15. We observe: **ReCL can slow down forgetting for non-homogenous neural networks.** For AlexNet, ReCL improves up to 4.44 % in terms of ACC, and up to 3 % for ResNet. These observations are interesting, as the theory underlying our framework is restricted to homogenous neural networks. It is therefore possible that parts of the theory might also extend to non-homogenous architectures. A detailed study is beyond the scope of this paper, and we thus leave it as an interesting direction for future research.

Table 15. **Scenario DIL:** Results for using our framework with AlexNet [28], a *none*-homogenous neural network violating the theoretical background of our framework. We nonetheless see improvements when adding ReCL. Shown: average ACC[↑], BWT[↑], and runtime over 5 random repetitions with varying task order and initializations. Complements Table 3 with runtimes.

Method	SplitCIFAR10	
	ACC	BWT
AlexNet	56.47	−31.63
AlexNet+ReCL	59.23	−28.25
AlexNet+ReCL (unsup.)	59.04	−28.24
AlexNet+ReCL (sup.)	57.03	−29.26
ResNet	53.53	−28.17
ResNet+ReCL	55.16	−29.41
ResNet+ReCL (unsup.)	56.41	−28.23
ResNet+ReCL (sup.)	53.51	−32.69

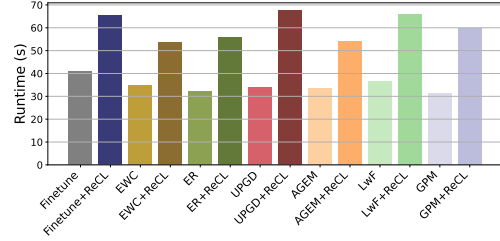


Figure 16. Runtimes for SplitMNIST.

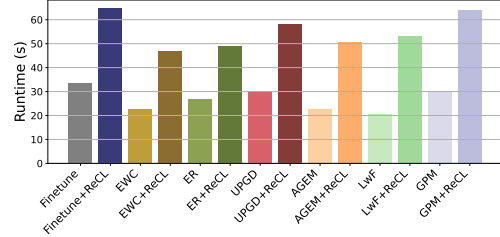


Figure 17. Runtimes for SplitTinyImageNet

K. Scalability Analysis

We visualize the runtimes for ReCL in Figures 16 and 17. We have the following observations: (1) The overhead for ReCL is relatively small. For example, the runtime of our Finetune+ReCL is roughly twice as long as the Finetune baseline. (2) The computational cost is largely insensitive to the dataset type. On SplitMNIST and SplitTinyImageNet, runtime increases are roughly similar. (3) The runtime of ReCL is insensitive to the underlying CL algorithm. For example, in Figure 16, all evaluated CL algorithms show similar runtime increases from our framework. (4) The *in-training* tuning strategies incur larger overheads (cf. Table 16). We thus recommend the naïve strategy for use in practice.

Table 16. **Runtime Analysis:** Runtimes on the SplitMNIST and SplitTinyImageNet datasets for the *unsupervised optimization strategy*.

Approach	MNIST	TinyImageNet
Finetune	40.71	33.32
Finetune+ReCL (unsup)	477.62	414.72
EWC	34.93	22.60
EWC+ReCL (unsup)	465.32	395.97
ER	31.96	26.81
ER+ReCL (unsup)	459.0	397.23
UPGD	33.82	30.05
UPGD+ReCL (unsup)	464.77	407.57
AGEM	33.54	22.50
AGEM+ReCL (unsup)	458.40	400.91
LwF	36.46	20.38
LwF+ReCL (unsup)	484.21	401.90